Geophys. J. R. astr. Soc. (1985) **82**, 1–30

Estimating explosion yield by analytical waveform comparison

Thorne Lay *Department of Geological Sciences, University of Michigan, 1006 C.C. Little Bldg, Ann Arbor, MI 48109, USA*

Accepted 1984 December 7. Received 1984 December 5, in original form 1984 July 16

Summary. The yields of 28 underground nuclear explosions at NTS (25 on Pahute Mesa) are estimated by applying a relative waveform analysis called intercorrelation to 1256 teleseismic short-period *P*-waves recorded at 74 WWSSN and CSN stations. Corrections for the effects of *pP* interference and yield-scaling of the explosion source functions are determined and applied to the waveforms, enabling analytical comparison of signals from events with different yields and burial depths. The procedure accounts for common receiver and propagation effects. Relative explosion source strengths in the 0.5–2.0 Hz frequency band are determined, with results of near-field modelling of strong ground motions establishing the absolute source spectral levels. Four events with detailed near-field models are used as master events in the intercorrelation process, and it is demonstrated that the relative source strengths are better resolved than the absolute values. Events with announced yields are used to determine empirical relations between yield and source strength, which in turn predict the yields of the other events. These yield estimates are shown to be comparable with those obtained by standard m_b and relative amplitude analysis. The analytical waveform comparisons also provide estimates of the *pP* parameters for each event, and criteria for identifying anomalous events, such as PIPKIN and MUENSTER, for which the waveforms differ from those of other events in the test site. Possible mechanisms affecting the anomalous events are considered. Pahute Mesa is shown to be a distinct subsite within NTS, with different teleseismic amplitude and waveform variations than observed at other subsites.

Introduction

The necessity of providing accurate (within 10 per cent) seismic yield estimates for underground nuclear explosions has spurred the development of new techniques that utilize more amplitude and waveform information than conventional parametric measurements such as m_b. It appears that standard m_b analysis cannot provide the desired accuracy due to the intrinsic complexity of short-period wave propagation in the Earth (Bache 1982). There is

some indication that alternate measurements such as spectral magnitudes (Shapira & Kulhanek 1978; Kraft, Griffin & Baumgardt 1982; Bache, Day & Savino 1979); coda magnitudes (Baumgardt 1983; Ringdal 1983); relative waveform comparisons (Mellman & Kaufman 1981; Lay, Burdick & Helmberger 1984a); or forward models (e.g. Bache *et al.* 1979) may provide more accurate yield estimates in certain cases. The latter techniques all attempt to reduce the influence of the poorly understood time domain amplitude fluctuations, which are ubiquitous for narrow band recordings. This is accomplished by extending the frequency band over which the waveform measurement is made. Of course such utilization of complete waveform information comes with the cost of requiring a more complete understanding of the source and propagation contributions to the signals.

One technique with potential for improving our yield estimation ability and understanding of events within a particular test site, is the intercorrelation procedure developed by Lay *et al.* (1984a, hereafter referred to as Paper 1). This relative waveform analysis involves analytical comparison of teleseismic short-period *P*-waves from two nuclear tests recorded at a given station. Differences in the two waveforms are mapped into a simple parameterization of the transfer function that differs between the events. If the events are of similar size and have epicentres sufficiently close together that the path and receiver properties are the same, the varying transfer function for each event can be idealized as a spike train consisting of *P* and *pP* arrivals. If the source sizes differ substantially, yield-scaled source functions must be included in the transfer functions. Additional complexity due to crustal reverberations or slapdown phases resulting from spall can be incorporated if necessary. The waveforms are equalized by convolving the observation for each event with the effective source function (consisting of the source time function convolved with the surface interaction spike train) for the other event, as shown in Fig. 1. By minimizing the waveform differences in the intercorrelated signals for a large number of stations simultaneously, the lag times and relative amplitudes of *pP* and the relative source strengths can be determined. In practice, one event is treated as a master event, for which a detailed source model is independently available.

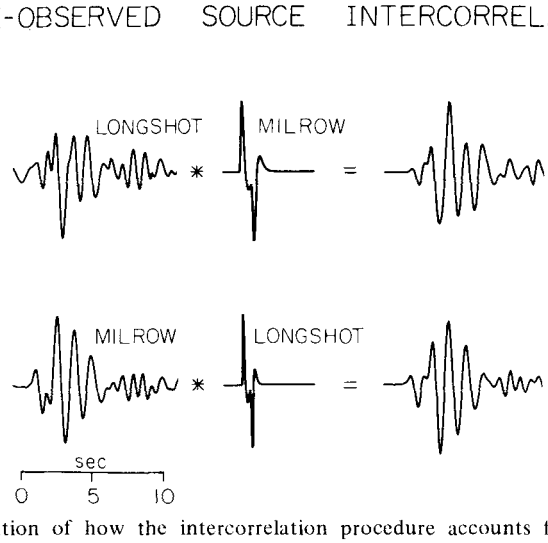

Figure 1. An illustration of how the intercorrelation procedure accounts for waveform differences produced by the source. In the top row the LONGSHOT observation at station ADE is convolved with the expected MILROW source function, which includes the *pP* arrival and the source time function. The bottom row shows the convolution of the MILROW observation at ADE with the LONGSHOT source function. The resulting signals are compared by cross-correlation. In practice this procedure is applied to many stations simultaneously.

This procedure directly accounts for common path and receiver effects without having to model them quantitatively, as is necessary for forward modelling techniques. The nature of the relative comparisons is such that differences in the effective source functions are better resolved than the absolute values of the parameters. This is actually beneficial, for it reduces the dependence of the results on the master event parameters, and enables large numbers of stations to be treated simultaneously.

The intercorrelation results can be used to predict yield by determining empirical relations between known yields and the source strengths derived in the passband of the data, or by direct use of yield-scaling relations, if such are sufficiently well known. In addition to yield estimates, intercorrelation provides complete high-frequency source models, and an objective means by which to detect events with anomalous *pP* behaviour or additional complexity not accounted for by the source function parameterization that was adopted. The latter application is essential to the process of defining 'distinct test sites' which are comprised of groups of events for which the relative yields can be reliably estimated. The cost for these gains is the need to have reliable source-time function representations with well-established yield-scaling behaviour, and soundly based models for the near-source surface interaction effects.

In Paper 1 the intercorrelation procedure was applied to the three underground nuclear explosions on Amchitka Island. For MILROW and CANNIKIN, the intercorrelation of a large number of WWSSN recordings gave source strength estimates in close agreement with results from near-field modelling. It was also demonstrated that using the simplest transfer function parameterization, with only *P* and *pP* arrivals and appropriate source time functions, was very successful in matching the waveforms of events with yields as different as CANNIKIN (< 5000 kt) and LONGSHOT (80 kt). When more complicated models that include a third arrival, mimicking a slapdown phase, are used, the *pP* parameters obtained are slightly different, but the source strength estimates are only changed by a few per cent. Thus, the *pP* parameters found by intercorrelation are considered to be 'effective' *pP* parameters, into which deficiencies of the source parameterization are folded. Nonetheless, for the Amchitka events the *pP* parameters derived in the analysis are in close agreement with independent spectral and forward modelling investigations, particularly for the *pP-P* lag time. This indicates the predominance of the *pP* interaction and shows that the simple source parameterization is quite realistic.

In this paper a large teleseismic short-period *P*-wave data set for NTS explosions is analysed using the intercorrelation procedure and standard m_b and relative amplitude analysis. The treatment of the data and application of the intercorrelation analysis follows the approach that would realistically be applied to analysis of events in a foreign test site, though only short-period data are used. Yield estimates from the intercorrelation and amplitude analyses are compared in lieu of having released yields for all of the events. Implications of the source models and distinct test site characteristics of NTS are considered.

Amplitude measurements and waveform data for NTS explosions

Short-period *P*-wave recordings from the 74 WWSSN and CSN (Canadian Seismic Network) stations shown in Fig. 2 were collected for 28 large NTS explosions. All but three of the events were located in Pahute Mesa, with the epicentres shown in Fig. 2. The other events are FAULTLESS (150 km north of Pahute Mesa), COMMODORE (Yucca Flat) and PILEDRIVER (Climax Stock). The ab (first peak-to-first trough) and bc (first trough-to-second peak) amplitudes were measured at each of the 71 stations in the distance range 25–98°, resulting in 1235 and 1240 reliable measurements respectively. The waveforms were

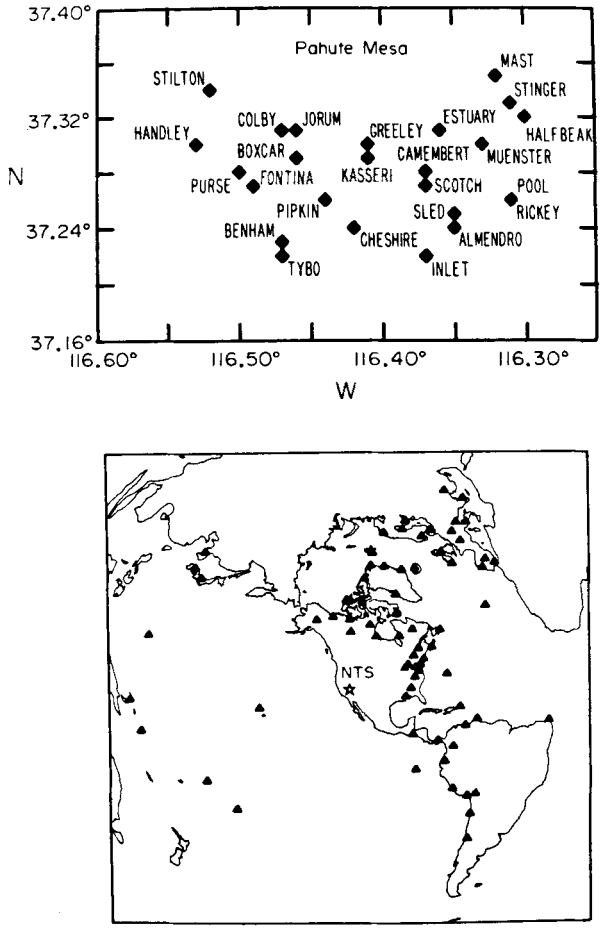

Figure 2. Top: Base map showing the locations of the 25 Pahute Mesa explosions for which teleseismic short-period *P*-waves have been measured and digitized. Bottom: The distribution of the 74 WWSSN and CSN stations in the distance range 15–98° from the NTS from which data were collected.

manually digitized whenever possible, yielding 1256 digitized signals. The waveforms for three stations at upper mantle distances (15–25°), SHA, PHC and FSJ, were digitized, but their amplitudes are not included in the amplitude analysis.

Due to the controversy over the most appropriate amplitude measurement to make, the ab and bc amplitudes are processed in three ways. The first procedure involves correcting the amplitudes only for the gain of the instrument at 1 s period, and applying geometric spreading corrections from Langston & Helmberger (1975) to equalize the distances to 50°. Measurements processed in this manner are labelled '*ab*' or '*bc*'. The period, *T*, of the first cycle of the *P* arrival was measured on the digitized waveforms, and these values are used to apply period-dependent instrument gain corrections to the *ab* and *bc* measurements along with the spreading corrections. These values are labelled 'A^{ab}' or 'A^{bc}' and are used to determine the ratios A^{ab}/T and A^{bc}/T. The third type of measurements are standard magnitudes:

$$m_b^{ab,\,bc} = \log \frac{(A^{ab,\,bc})}{T} + p\,(\Delta)$$

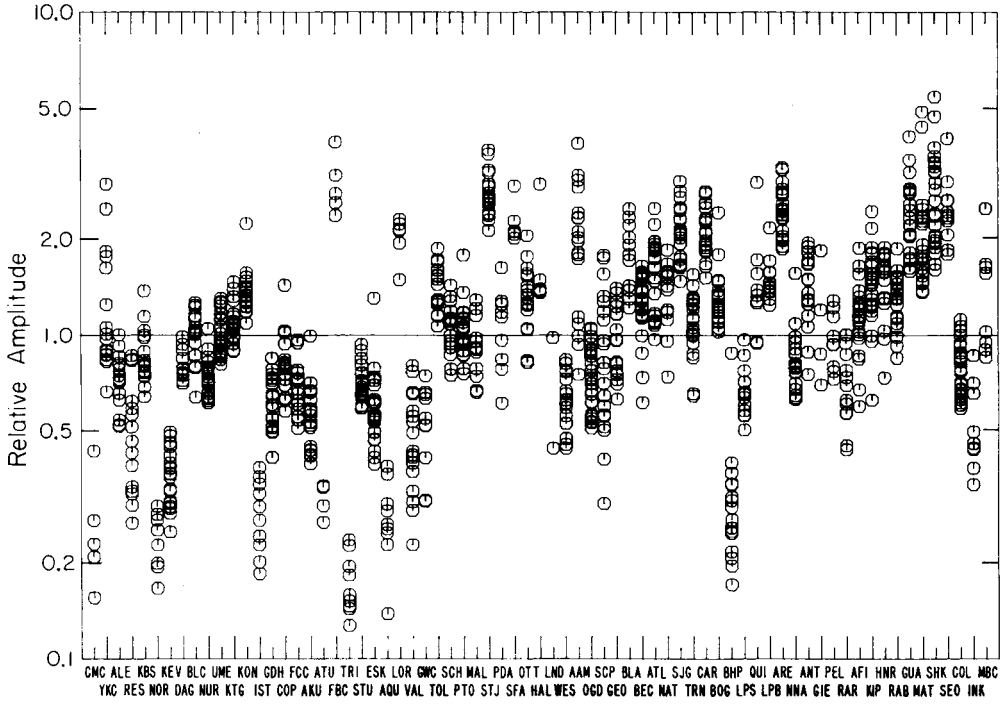

Figure 3. The complete short-period *P*-wave *ab* amplitude data set for 25 Pahute Mesa events after applying event size corrections. The stations are ordered by azimuth from the test site. The 1096 amplitudes have been corrected for geometric spreading to a distance of 50°.

where $p(\Delta)$ are the distance factors of Veith & Clawson (1972). The geometric spreading corrections were not applied to $A^{ab,\,bc}$ in the magnitude calculations. All of the amplitude measurements and waveforms can be found in Lay *et al.* (1984c, e). For all 28 events in this study, the apparent *pP* delay times are greater than 0.7 s, thus the '*ab*' type measurements are generally measures of the direct *P* arrival alone, while the '*bc*' type measurements are influenced by *pP* interference, which varies from event to event. Thus, we anticipate a high degree of correlation between source strength estimates from '*ab*' measurements and the intercorrelation results, for this set of events.

Station-path corrections for each of the six types of amplitude measurements were established using the 25 Pahute Mesa events. The path corrections were obtained after first determining event size corrections by the least squares procedure described by Butler & Ruff (1980). Fig. 3 shows the 1096 *ab* amplitudes involved in this procedure, after applying the event corrections. The small scatter at each station shows that, to first order, the Pahute Mesa events all have the same basic amplitude pattern. Stations TRI and BHP have anomalous waveforms, with small percursory arrivals for which the *ab* amplitudes are not comparable measures of the waveform with those at other stations. The station averages for the 71 stations, normalized to have an overall mean value of 1 (or 0, for the magnitude corrections), are taken to be station-path corrections. These path corrections show a clear azimuthal pattern. European and Canadian stations at azimuths from due north to N45°E record amplitudes that are 2–3 times smaller than signals at other azimuths. This systematic azimuthal variation is discussed in detail by Lay, Wallace & Helmberger (1984b). The path corrections for each type of amplitude measurement are tabulated in Lay *et al.* (1984e).

Table 1. Average amplitude measurements with path corrections.*

Event	Date	Depth, km	ab, mμ	$\frac{A^{ab}}{T}$, mμ/s	m_b^{ab}	n^{ab}	bc, mμ	$\frac{A^{bc}}{T}$, mμ/s	m_b^{bc}	n^{bc}
ALMENDRO	6/06/73	1.064	370±72	416±72	5.96±0.10	45	535±91	607±120	6.13±0.09	44
BENHAM	12/19/68	1.402	505±100	643±145	6.16±0.09	49	746±135	945±194	6.33±0.09	47
BOXCAR	4/26/68	1.158	472±100	595±148	6.12±0.11	47	668±145	840±190	6.27±0.10	47
CAMEMBERT	6/26/75	1.311	416±52	501±78	6.05±0.07	45	590±105	713±136	6.21±0.09	44
CHESHIRE	2/14/76	1.167	229±52	256±64	5.76±0.10	36	315±91	353±104	5.89±0.12	36
COLBY	3/14/76	1.273	596±109	748±172	6.22±0.10	43	796±166	1011±250	6.35±0.10	40
ESTUARY	3/09/76	0.869	187±27	222±47	5.70±0.09	33	268±46	319±66	5.85±0.09	33
FONTINA	2/12/76	1.219	516±92	683±133	6.19±0.08	38	674±136	894±173	6.30±0.08	38
GREELEY	12/20/66	1.215	422±105	550±150	6.09±0.11	61	592±133	776±187	6.24±0.12	61
HALFBEAK	6/30/66	0.819	251±54	286±57	5.81±0.09	47	386±81	443±95	6.00±0.10	48
HANDLEY	3/26/70	1.206	703±190	980±298	6.34±0.12	53	937±210	1315±339	6.47±0.11	52
INLET	11/20/75	0.817	210±57	228±58	5.71±0.11	39	314±88	342±93	5.88±0.12	40
JORUM	9/16/69	1.158	484±97	649±150	6.16±0.10	57	701±139	942±217	6.32±0.10	57
KASSERI	10/28/75	1.265	493±106	629±169	6.14±0.11	41	683±120	868±196	6.29±0.10	40
MAST	6/19/75	0.912	253±59	288±75	5.81±0.12	53	380±85	437±117	5.99±0.12	53
MUENSTER	1/03/76	1.451	484±103	576±148	6.11±0.11	40	710±152	851±217	6.28±0.11	40
PIPKIN	10/08/69	0.617	81±17	93±26	5.31±0.11	42	123±30	140±40	5.49±0.11	42
POOL	3/17/76	0.879	246±59	268±67	5.78±0.11	36	358±83	392±91	5.94±0.11	38
PURSE	5/07/69	0.599	123±32	144±37	5.51±0.12	48	193±46	225±51	5.70±0.10	48
RICKEY	6/15/68	0.683	146±37	161±39	5.56±0.10	30	242±58	267±55	5.78±0.09	31
SCOTCH	5/23/67	0.978	104±24	110±35	5.39±0.11	38	156±33	166±50	5.57±0.11	38
SLED	8/29/68	0.729	217±64	251±79	5.75±0.12	41	311±104	356±118	5.90±0.13	45
STILTON	6/03/75	0.731	156±44	175±53	5.59±0.12	47	244±69	275±84	5.78±0.12	47
STINGER	3/22/68	0.668	85±29	101±37	5.35±0.14	37	145±39	172±53	5.58±0.13	39
TYBO	5/14/75	0.765	242±45	285±61	5.81±0.09	50	361±80	427±110	5.98±0.11	51
COMMODORE**	5/20/67	0.746	167±117	200±133	5.66±0.27	51	239±158	289±184	5.85±0.25	51
FAULTLESS**	1/19/68	0.975	411±230	602±342	6.18±0.25	57	684±370	1001±555	6.41±0.25	57
PILEDRIVER**	6/02/66	0.500	101±77	114±83	5.41±0.29	31	145±133	165±148	5.54±0.35	33

* Error estimates are standard deviations.

** No path corrections.

The application of period corrections in the amplitude measurements does not significantly affect the scatter in the station values.

The mean amplitude for each event was computed using the path corrections as weighting factors. This process eliminates the need to average the observations azimuthally or to use

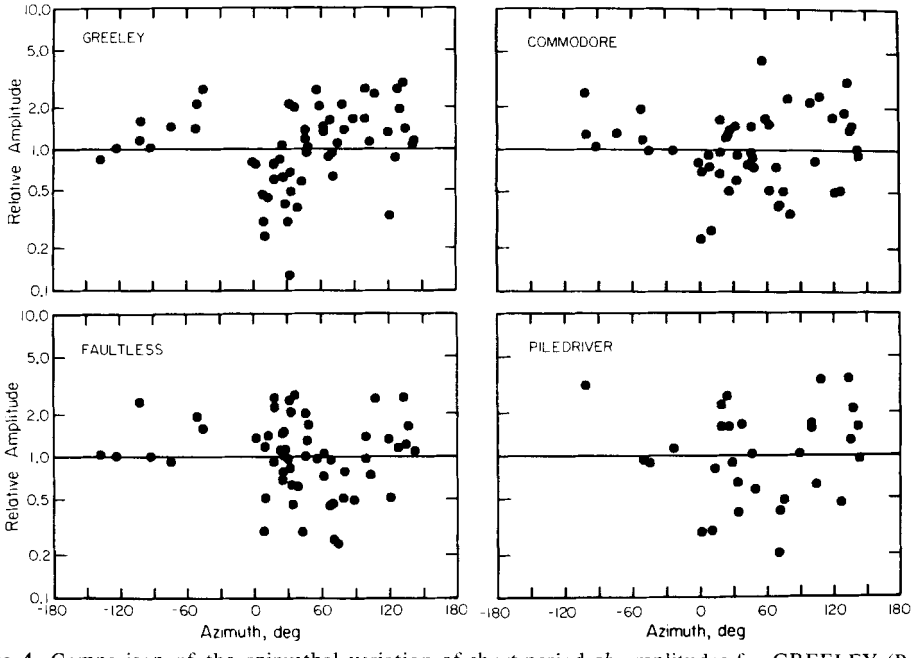

Figure 4. Comparison of the azimuthal variation of short-period *ab* amplitudes for GREELEY (Pahute Mesa), FAULTLESS (150 km north of Pahute Mesa), COMMODORE (Yucca Flat) and PILEDRIVER (Climax Stock).

maximum likelihood estimates to account for incomplete sampling. Table 1 lists the resulting mean and standard deviation for each measurement for the 25 Pahute Mesa events. The m_b^{bc} values are close to the m_b values reported by the ISC. Without the path corrections, the average standard deviation for the m_b^{ab} and m_b^{bc} values are 0.26 and 0.27 respectively, whereas after applying the corrections they are 0.11 in both cases. This factor of 2.5 reduction in the standard deviation is typical of that attained when path corrections are applied for a single test site (Bache 1982). The mean m_b values changed only in the second decimal place when the corrections were applied, due to the large number of observations for each event. Mean amplitude values for the three non-Pahute Mesa events are included in Table 1, with no path corrections being applied. Applying the Pahute Mesa path corrections actually increases the standard deviation for $m_b^{ab,\,bc}$ for FAULTLESS, and only slightly decreases those for PILEDRIVER and COMMODORE. Fig. 4 shows that the azimuthal amplitude pattern for Pahute Mesa differs significantly from those of the other three events.

The NTS observations also show significant waveform variations. The short-period *P*-waves recorded at WWSSN stations UME and OGD for several Pahute Mesa events, as well

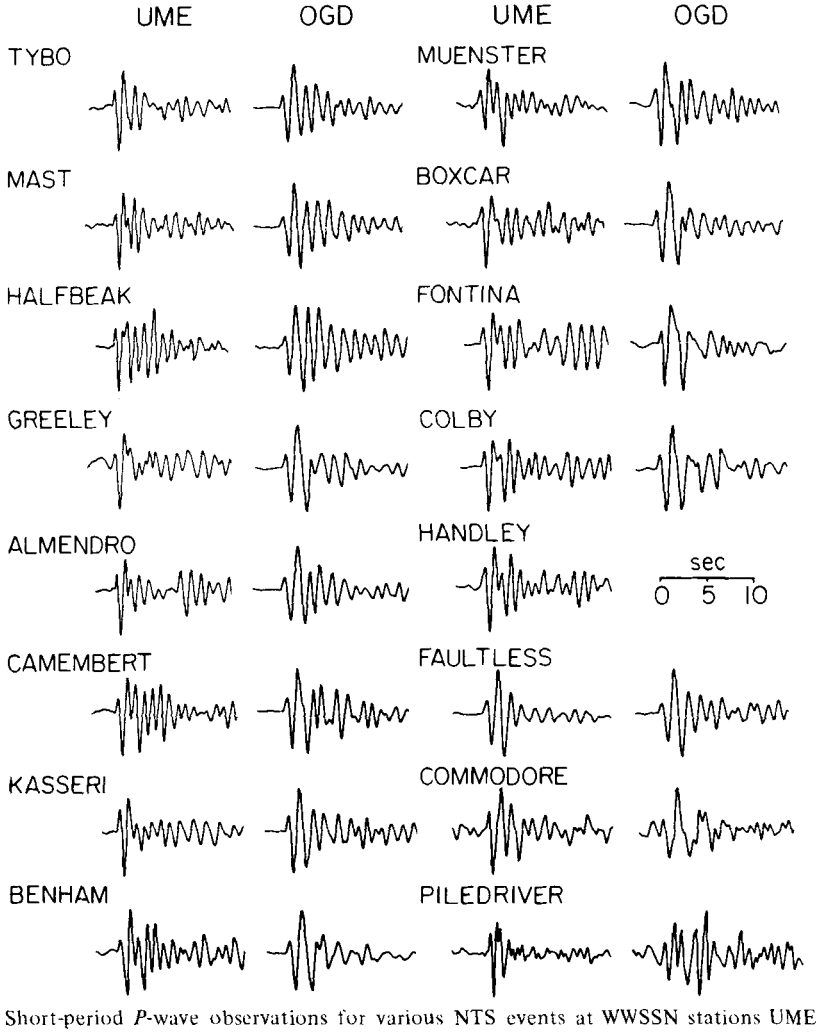

Figure 5. Short-period *P*-wave observations for various NTS events at WWSSN stations UME (N 19° E) and OGD (N70° E). The peak amplitudes are normalized to unity.

as for FAULTLESS, COMMODORE and PILEDRIVER are shown in Fig. 5. UME lies at an azimuth of N19° E while OGD is at N70° E. It is interesting to note that these stations record similar waveforms for FAULTLESS, but very different waveforms for the other events. PILEDRIVER and COMMODORE have distinctive waveforms. Among the Pahute Mesa events, HALFBEAK and CAMEMBERT have more complicated codas in the first 5 s after the *P* arrival, while the UME recording of MUENSTER has an unusually strong third downswing. There is less variation in the signals at OGD, which records lower frequency signals than UME. These variations are clearly the result of many phenomena, including the different source functions, the receiver functions, near source velocity structure, complex surface interactions, and intrinsic scattering properties along the paths. The variations apparent throughout the waveforms suggest that the *ab* or *bc* amplitudes are varying substantially as well. Part of the purpose of this study is to address whether these variations are deterministic and can be objectively accounted for, or whether they are stochastic to a degree that precludes the quantitative use of short-period waveforms.

Intercorrelation of NTS events

In applying the intercorrelation procedure to the NTS data, an approach was followed that would realistically be applied to events from a foreign test site. That is, given detailed information about the yields and source functions for several master events (in the present case these are obtained from near-field modelling of strong ground motions) and large teleseismic short-period *P*-wave data sets for the master and unknown events, the intercorrelation procedure is applied to correct the signals for the effects of surface interaction and corner frequency scaling, and the unknown source strengths are determined. In order to attain the best understanding of each source, it is envisioned that long-period *P*-, *pS*-, Rayleigh- and Love-waves recorded for each event would be analysed simultaneously by both intercorrelation and conventional analysis. Only short-period data are used in this study.

A major advantage of applying the intercorrelation procedure to Pahute Mesa events is that, as was the case for the analysis of Amchitka events in Paper 1, near-field strong ground motion velocity records for several of the events have been modelled by Hartzell, Burdick & Lay (1983). They used a modified Haskell source representation given by

$$\psi(t) = \psi_\infty [\![1 - \exp(-Kt)[1 + Kt + (Kt)^2/2 - B(Kt)^3]]\!] \quad (1)$$

where ψ_∞ is the DC level source strength, K is the rise time parameter, and B governs the time function overshoot. The validity of this source function for modelling broadband data for underground nuclear explosions has been demonstrated by Burdick, Wallace & Lay (1984) and Lay, Helmberger & Harkrider (1984d). The near-field models establish the absolute values of the source parameters for several master events. While values of K can be well-resolved once an appropriate source region velocity structure is determined, B and ψ_∞ trade-off directly in the high-frequency near-field data. Hartzell *et al.* (1983) set $B = 1$ and determined corresponding values of ψ_∞, which thus may not be the actual DC level source strength if the true value of B is different or if it varies with yield. Paper 1 discussed this trade-off at length, because the intercorrelation procedure has a similar trade-off, as long as narrow band signals are used. Throughout this paper all values of ψ_∞ are appropriate for $B = 1$, and indicate the source strength in the pass-band of the data (0.5–2 Hz). While the intercorrelation procedure is intrinsically a relative waveform analysis, and absolute source strengths are not required for determining relative source strengths, it is important to know the appropriate corner-frequency behaviour for a given test site.

Hartzell *et al.* (1983) determined the source parameters listed in Table 2 for six Pahute Mesa events. Using these parameters to predict average observed teleseismic *ab* amplitudes

Table 2. Near field source models ($B = 1$).

Event	Depth, m	K	ψ_∞ ($\times 10^{10}$ cm^3)
BOXCAR	1160	7	13
MAST	912	8	4.3
INLET	817	9	3.0
SCOTCH	970	10	1.4
HANDLEY	1200	6	16
JORUM	1160	6	15

for each event leads to average t^* values varying from 0.66 to 0.88 s. MAST, INLET and SCOTCH give consistent values near 0.7 s, while the other events give larger t^* values. This could result from several factors, including variable velocity structure in the Mesa, anomalously low teleseismic amplitudes for the larger events, or inflated ψ_∞ values for the larger events due to non-linear contributions to the near-field velocity amplitudes. The models for JORUM and HANDLEY are based on inferior quality data, so the other four events will be used as master events in the intercorrelation analysis.

In using the source function (1) in the intercorrelation of events with different yields, it is necessary to specify or determine values of K. Since K trades-off strongly with pP lag, it is not possible to determine both by intercorrelation. A simple procedure for estimating K is adopted here, which is free of uncertainties in source scaling laws and t^*. A log-log regression provided an empirical relation between the near-field determinations of K for the four master events and their teleseismic P-wave amplitudes, as measured by the inverse ab amplitude event size factors, α^{-1}, described in the previous section. The resulting expression is

$$\log K = (0.848 \pm 0.014) - (0.223 \pm 0.034) \log (\alpha^{-1}) \tag{2}$$

which gives the K values listed in Table 3. Using any of the alternate average amplitude estimates given in Table 1 results in similar values of K with amplitude scaling exponents of -0.22 to -0.25. K values for the non-Pahute Mesa events were selected on the basis of their relative ab amplitudes. It was shown in Paper 1 that an error in K of 10–20 per cent produces only a few per cent error in ψ_∞ determinations, for K values of 10 and larger and using WWSSN data in the intercorrelation procedure.

The empirical relation given by (2) is actually close to the prediction of the Mueller & Murphy (1971) model which gives K as a function of depth, h, and yield, Y:

$$K \alpha h^{0.42} / Y^{1/3}. \tag{3}$$

Assuming normal depth scaling with yield:

$$h \alpha Y^{1/3} \tag{4}$$

along with equation (3) results in

$$K \alpha Y^{-0.19}. \tag{5}$$

Taking Murphy's (1977) relation between yield and amplitude

$$m_b = 0.85 \log Y \tag{6}$$

predicts K scaling of the form

$$\log K \alpha - 0.22 m_b. \tag{7}$$

Table 3. Empirical estimation of K.

Event	Event Factor, α_i^{-1}	K obs*	K
PIPKIN	0.161		10.6
STINGER	0.165		10.6
SCOTCH	0.195	10.0	10.2
PURSE	0.239		9.7
STILTON	0.313		9.2
RICKEY	0.329		9.1
ESTUARY	0.361		8.9
INLET	0.413	9.0	8.6
SLED	0.450		8.4
CHESHIRE	0.454		8.4
TYBO	0.487		8.3
MAST	0.509	8.0	8.2
POOL	0.514		8.2
HALFBEAK	0.529		8.1
GREELEY	0.778		7.5
ALMENDRO	0.780		7.5
CAMEMBERT	0.859		7.3
JORUM	0.947	(6.0)	7.1
KASSERI	0.958		7.1
BENHAM	0.987		7.1
MUENSTER	0.999		7.1
BOXCAR	1.000	7.0	7.1
FONTINA	1.064		7.0
COLBY	1.194		6.8
HANDLEY	1.403	(6.0)	6.6
FAULTLESS			7.1
PILEDRIVER			10.2
COMMODORE			9.1

* From near-field modelling.
( ) Not used to establish the $K - \alpha_i^{-1}$ relation.

The amplitude measurements in this paper are shown below to have yield-scaling exponents from 0.77 to 0.92, which are generally consistent with (6).

Keeping $B = 1$ and using the K values in Table 3, the intercorrelation procedure is applied here to determine ψ_∞, pP-P lag time, and pP/P amplitude for each of the Pahute Mesa events. We follow the same procedure used in Paper 1 of adopting a reference event, specifying its pP parameters, and then stepping through the pP parameter space for the secondary event. As in Paper 1, two norms are used to appraise the intercorrelations for each case. The first is a waveform norm given by

$$N_w = \frac{1}{n}\sum_{i}^{n}(1 - \mathrm{ccc}_i) \tag{8}$$

where n is the number of stations and ccc_i is the optimal lag normalized cross-correlation coefficient for the ith station intercorrelation. This norm is minimized for the best selection of pP parameters. The second norm is used to determine the unknown ψ_∞ since it retains the absolute amplitude information. It is given by the optimal cross-correlation lag time integral

$$N_a = \frac{1}{n}\sum_{i}^{n} w_i \int_t [I_i(t) - J_i(t)]^2 dt, \tag{9}$$

where $I_i(t)$ is the convolution of the seismogram recorded at station i for the first event with the source function of the second event, and $J_i(t)$ is the convolution of the seismogram recorded at station i for the second event with the source function for the first event. The w_i are weights applied to give uniform contribution for each station, and are here taken to be the inverse square of the ab path correction for each station. N_A is minimized for the optimal ψ_∞ for the second event.

To specify the *pP* parameters for the reference events we have used as starting values the *pP* delays for BOXCAR and SCOTCH given by Springer (1974). These delays are estimated from surface recordings near the shot points indicating the arrival time of the upgoing *P*-waves. Similar information would probably be available for a calibration shot, otherwise spectral techniques can provide *pP* delays from teleseismic data. An elastic *pP* reflection coefficient of -0.9 is used for each master event. This is the simplest assumption to make and worked very successfully for the Amchitka analysis in Paper 1. When smaller reflection coefficients were assumed in that study there was little, if any, improvement in N_W, and the resulting ψ_∞ values vary by only a few per cent. Recalling that the intercorrelation analysis is most sensitive to *differences* in *pP* parameters between events, these selections are not extremely critical, though the particular values are realistic. As a test of the *pP* delays given by Springer, we performed an intercorrelation of 18 pairs of waveforms for GREELEY and SCOTCH. A *pP* delay of 0.97 s, given by Springer (1974), was used for the former event, and the *pP* delay for SCOTCH was determined by minimizing the waveform norm. SCOTCH has a yield of 155 kt and was overburied at a depth of 978 m. GREELEY was buried at a depth of 1215 m. Springer (1974) gives a SCOTCH *pP* delay of 0.91 s, close to that for GREELEY. The best *pP* delay found for SCOTCH is 0.95 s, which compares well with Springer's (1974) result. A similar test using BOXCAR and its *pP* delay (0.96 s) given by Springer (1974) gives the same result for SCOTCH. This indicates that a *pP* delay of 0.95 s is valid for SCOTCH, and Springer's (1974) value of 0.96 s for BOXCAR is also used. While these delays are not necessarily the true average delays, they are compatible with the near-in surface records.

The first set of intercorrelations was performed with SCOTCH as a master event, with the following fixed parameters: $pP\text{-}P = 0.95$ s, $|pP|/|P| = 0.9$, $K = 10.0$, $B = 1$, $\psi_\infty = 1.4 \times 10^{10}\,\mathrm{cm}^3$. Intercorrelations were performed with each of the other 24 Pahute Mesa events and FAULTLESS, COMMODORE and PILEDRIVER. The non-Pahute Mesa tests were treated exactly the same as the other events. These intercorrelations involved between 16 and 40 pairs of traces. A parameter search was conducted for *pP* parameters of the secondary events covering the range $pP\text{-}P = 0.7$–1.25 s and $|pP|/|P| = 0.3$–1.5. In every case a minimum in the waveform norm (8) was found giving the preferred *pP* parameters, and, for that selection, ψ_∞ was determined by minimizing the amplitude norm (9). The intercorrelated waveforms for the optimal *pP* parameters in the SCOTCH:GREELEY intercorrelation are shown in Fig. 6. The cross-correlation coefficients are very comparable to those for the MILROW:LONGSHOT intercorrelation described in Paper 1, with a similar overall waveform norm (0.156 versus 0.166 for MILROW:LONGSHOT). A 7 s time window, which spans the first 5 s of the original waveforms, was used for the intercorrelations, as was adopted in Paper 1. Fig. 7 shows the sensitivity of the waveform norm to the *pP* parameters for GREELEY in this intercorrelation, along with the dependence of the ψ_∞ estimate for GREELEY on the *pP* parameters. As was found in Paper 1, the *pP* delay is better resolved than the $|pP|/|P|$ ratio, and the uncertainty in ψ_∞ resulting from uncertainty in the *pP* parameters for GREELEY is about 10 per cent.

Similar intercorrelations using SCOTCH as a master event yielded the results in Table 4. In most cases the waveform norm is less than 0.2, implying an average cross-correlation coefficient of 0.8 or greater. The largest waveform mismatches are for PILEDRIVER, PIPKIN and MUENSTER. In every case the waveform norm is lower than for the CANNIKIN:LONGSHOT intercorrelation in Paper 1 (0.30). The events with anomalous *pP* parameters are ESTUARY ($|pP|/|P| = 1.5$), COMMODORE ($|pP|/|P| = 1.5$), and MUENSTER ($pP\text{-}P = 1.3$ s). Previous estimates of *pP* delays for Pahute Mesa events are listed in Table 5, with those given by Springer (1974) being very consistent with the values in Table 4. The *pP* delays found for these intercorrelations are plotted as a function of source

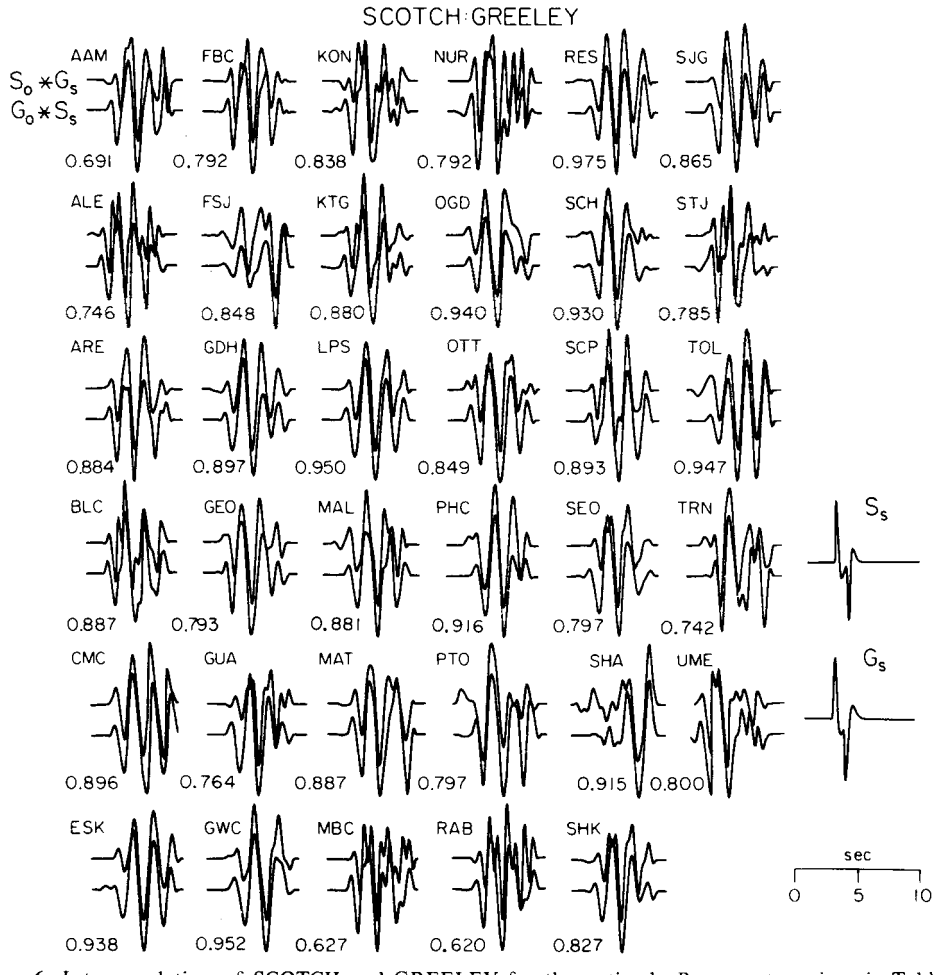

Figure 6. Intercorrelation of SCOTCH and GREELEY for the optimal *pP* parameters given in Table 4. The top trace in each pair is the SCOTCH observation, S_0, convolved with the GREELEY effective source function, G_s, and the lower trace is the GREELEY observation, G_0, convolved with the SCOTCH source function, S_s. The normalized cross-correlation coefficients for each station are shown below each trace pair. The effective source functions are shown on the right. $K = 10$ for SCOTCH and $K = 7.5$ for GREELEY.

depth in Fig. 8. A slight increase in delay is observed as a function of depth, and only MUENSTER appears to be clearly anomalous. Since all of these delays are longer than predicted for the known overburden velocities, it is not surprising to find scatter in the figure.

While the overall waveform norms for each intercorrelation are generally quite low, which is encouraging because it supports the simple source model adopted, it is of interest to investigate the residual misfit further. Fig. 9 shows the average waveform norms for the SCOTCH intercorrelations as a function of distance between the intercorrelated events. There is little indication of a separation distance influence for this case. The waveform norm for FAULTLESS is remarkably low considering its distance from SCOTCH, as well as the strong relative amplitude variation between FAULTLESS and Pahute Mesa events seen in Fig. 4; nor is there a clear relation between the waveform norm and relative source strength. One might expect events with similar yields to correlate better because of the similarity in K and *pP* delay, but this does not appear to be the case. For example, JORUM and

N_W |pP|/|P|

pP–P, sec	0.3	0.4	0.5	0.6	0.7	0.8	0.9	1.0
0.70	0.2353	0.2313	0.2284	0.2270	0.2260	0.2263	0.2273	0.2287
0.75	0.2122	0.2034	0.1972	0.1926	0.1897	0.1883	0.1881	0.1887
0.80	0.2011	0.1899	0.1822	0.1773	0.1742	0.1726	0.1722	0.1726
0.85	0.1972	0.1852	0.1770	0.1717	0.1688	0.1675	0.1676	0.1684
0.90	0.1929	0.1795	0.1701	0.1634	0.1592	0.1572	0.1564	0.1569
0.95	0.1934	0.1802	0.1704	0.1637	0.1593	0.1568	0.1562*	0.1566
1.00	0.2001	0.1876	0.1775	0.1704	0.1657	0.1631	0.1624	0.1631
1.05	0.2080	0.1957	0.1862	0.1797	0.1751	0.1728	0.1727	0.1740

$\psi_\infty \cdot 10^{10}$ CM^3

pP–P, sec	0.3	0.4	0.5	0.6	0.7	0.8	0.9	1.0
0.70	6.32	6.01	5.71	5.41	5.14	4.87	4.62	4.39
0.75	6.52	6.24	5.95	5.67	5.39	5.12	4.86	4.63
0.80	6.64	6.37	6.09	5.80	5.52	5.25	4.99	4.75
0.85	6.69	6.43	6.15	5.86	5.58	5.30	5.04	4.80
0.90	6.80	6.56	6.29	6.01	5.73	5.45	5.19	4.94
0.95	6.83	6.60	6.33	6.05	5.77	5.49	5.23*	4.97
1.00	6.90	6.69	6.44	6.17	5.90	5.63	5.36	5.11
1.05	6.95	6.75	6.52	6.26	6.00	6.73	5.46	5.20

Figure 7. The waveform norm is shown as a function of *pP* parameters for GREELEY for the SCOTCH:GREELEY intercorrelation (top), and the GREELEY source strength, ψ_∞, is shown for each case (bottom). The asterisks indicate the preferred *pP* parameters and the corresponding optimal ψ_∞.

BOXCAR have lower waveform norms than STILTON and RICKEY. This may reflect the overburial of SCOTCH, which results in a *pP* lag time close to those of the larger events.

The individual station cross-correlation coefficients for the SCOTCH : GREELEY and SCOTCH : MUENSTER optimal intercorrelations are plotted as a function of azimuth from

Table 4. Intercorrelations with SCOTCH as master event.

(SCOTCH pP–P = 0.95 s, pP/P = 0.9, ψ_∞ = 1.4x10^{10} cm^3)

Event	NSTA	N_W	pP–P, s	pP/P	ψ_∞(x10^{10} cm^3)
ALMENDRO	28	0.1237	0.95	0.8	4.24
BENHAM	23	0.1981	0.90	0.8	6.73
BOXCAR	29	0.1237	0.95	1.0	5.86
CAMEMBERT	24	0.2045	1.00	0.6	4.62
CHESHIRE	28	0.1658	1.00	1.0	2.12
COLBY	24	0.2193	1.05	1.2	5.27
ESTUARY	21	0.1257	0.95	1.5	1.90
FONTINA	24	0.2138	0.90	0.9	4.58
GREELEY	35	0.1562	0.95	0.9	5.23
HALFBEAK	29	0.1373	0.85	1.1	3.02
HANDLEY	26	0.1428	0.95	0.7	8.66
INLET	26	0.1854	0.90	0.8	2.26
JORUM	26	0.1079	0.90	1.0	5.98
KASSERI	23	0.1600	0.90	0.8	5.54
MAST	34	0.1709	0.85	0.6	3.37
MUENSTER	22	0.2460	1.30	0.8	5.42
PIPKIN	27	0.2744	0.80	0.7	0.74
POOL	22	0.1322	0.95	1.1	2.49
PURSE	32	0.1899	0.80	1.0	1.30
RICKEY	16	0.1766	0.75	1.1	1.40
SLED	28	0.1490	0.85	0.9	1.98
STILTON	32	0.2271	0.85	0.7	1.54
STINGER	33	0.1972	0.80	1.2	1.02
TYBO	32	0.1522	0.85	0.8	3.04
FAULTLESS	33	0.1559	0.80	1.0	5.89
COMMODORE	40	0.2057	0.85	1.5	1.34
PILEDRIVER	22	0.2879	0.80	0.8	0.70

Table 5. Published estimates of *pP* delay time, s.

	Kulhanek (1971)	Marshall (1972)	Frasier (1972)	Springer (1974)
BENHAM	1.13			
BOXCAR	1.12		1.1	0.96
COMMODORE	1.03			0.84
FAULTLESS	1.02		0.9	0.80
GREELEY	1.07	1.0		0.97
HALFBEAK	0.92			0.72
HANDLEY			1.15	0.95
JORUM				0.98
PILEDRIVER	0.85	0.68		0.24
PURSE			0.75	
SCOTCH				0.91
STINGER			0.85	

NTS in Fig. 10. The distance separating the events in each case is the same; however, the average waveform norm for the SCOTCH : MUENSTER intercorrelation is significantly higher. This is apparent in Fig. 10, where stations at azimuths from 60° to 120° have lower cross-correlation coefficients for the SCOTCH : MUENSTER intercorrelation than stations at

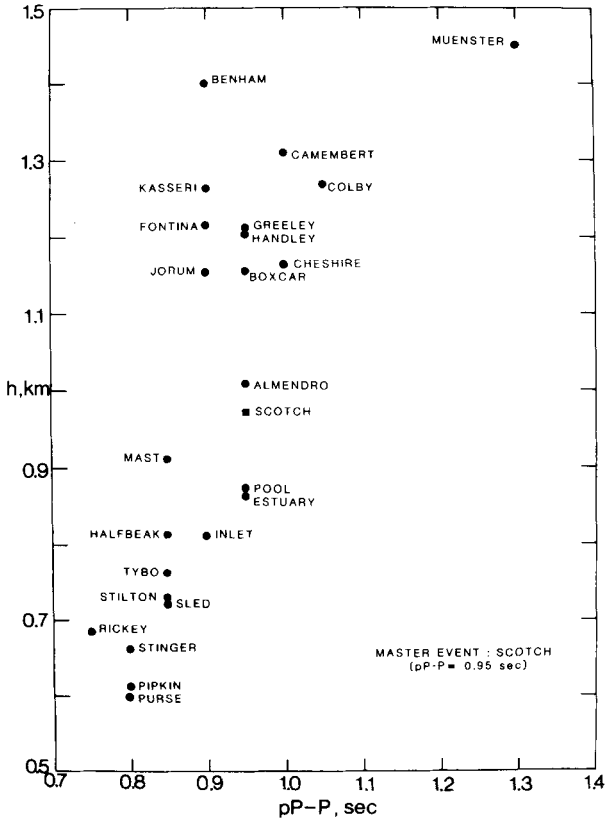

Figure 8. Comparisons of *pP* delay times found in the intercorrelations with SCOTCH as a master event with known burial depths, *h*.

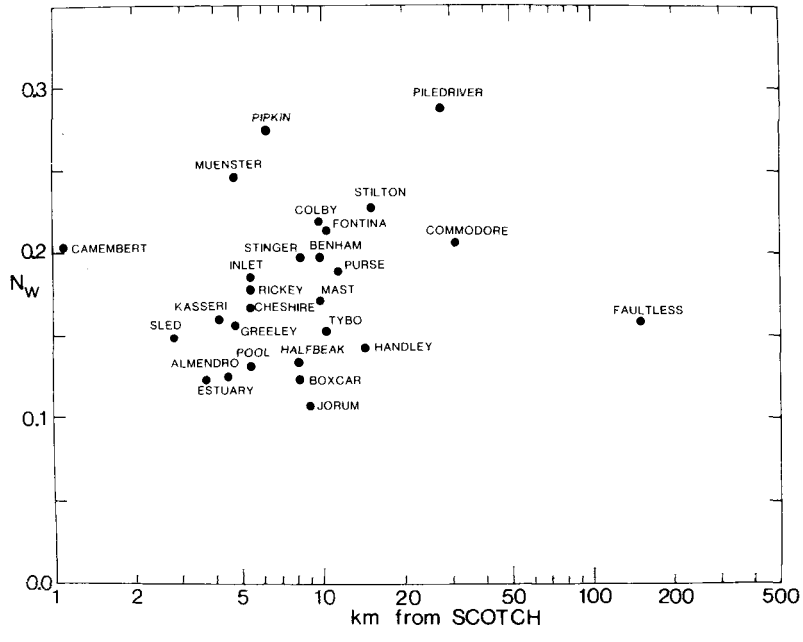

Figure 9. The waveform norms for the intercorrelations with SCOTCH as a master event plotted as a function of separation distance between the intercorrelated events.

similar azimuths for the SCOTCH : GREELEY intercorrelation. The anomalously large delay time found for MUENSTER (1.3 s) may be the result of this azimuthal variation of the *P* waveforms.

The next set of intercorrelations was performed with BOXCAR as a master event. The source parameters for BOXCAR were fixed at $pP–P = 0.96$ s, $|pP|/|P| = 0.9$, $K = 7$, $B = 1$, $\psi_\infty = 1.3 \times 10^{11}$ cm^3. A parameter search was performed to determine ψ_∞ and *pP* parameters for each of the other events. A 7 s time window was again used. Since BOXCAR has a longer-period source function, the intercorrelated waveforms are more heavily filtered than when SCOTCH is used as a reference event. This is illustrated in Fig. 11, which shows the waveforms for the optimal BOXCAR : GREELEY intercorrelation. Note that the normalized cross-correlation coefficients tend to be higher than for the SCOTCH : GREELEY intercorrelations, and the traces are generally smoother. The results of all 27 intercorrelations

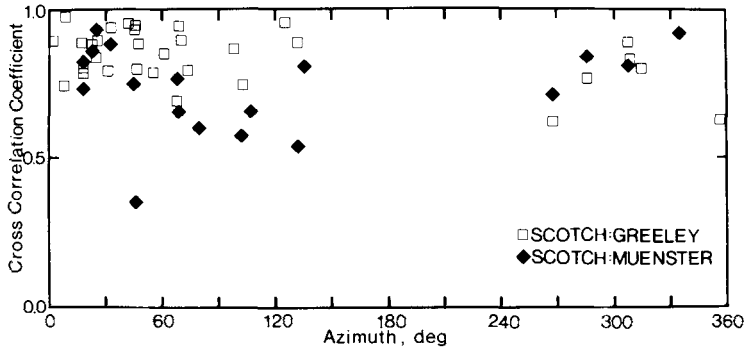

Figure 10. Individual station normalized cross-correlation coefficients for the SCOTCH : GREELEY and SCOTCH : MUENSTER intercorrelations plotted as a function of azimuth from NTS.

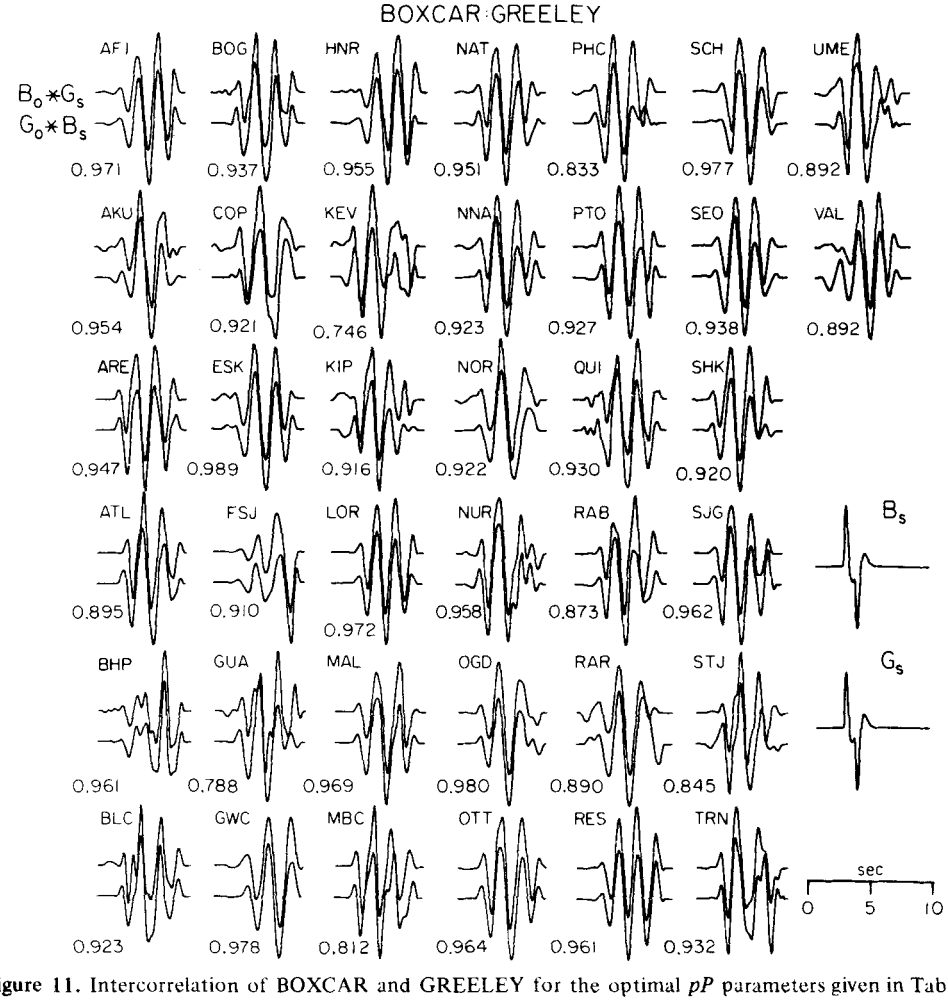

Figure 11. Intercorrelation of BOXCAR and GREELEY for the optimal *pP* parameters given in Table 6. The conventions are the same as in Fig. 6. $K = 7$ for BOXCAR and $K = 7.5$ for GREELEY.

with BOXCAR as a master event are listed in Table 6. The longer-period character of the intercorrelated waveforms appears to give less resolution of *pP* delay times, though the results are generally comparable to those found in the SCOTCH intercorrelations. MUENSTER again has an anomalously large *pP* delay time. Note that the ψ_∞ estimates are uniformly larger than those found for the SCOTCH intercorrelations, which will be discussed in detail below. Plotting the waveform norms as a function of distance between BOXCAR and the secondary events reveals a clear tendency for the residual misfit to increase with separation distance as shown in Fig. 12. Events PIPKIN and PURSE are relatively nearby but have large residual misfits, which may partially be due to their large difference in yield from BOXCAR. FAULTLESS again has a surprisingly low waveform mismatch.

When INLET was used as a master event, a *pP* delay of 0.90 s was adopted, which was determined by the SCOTCH : INLET intercorrelation. The other INLET source parameters were $|pP|/|P| = 0.9$, $K = 9.0$, $B = 1$, $\psi_\infty = 3.0 \times 10^{10}\,\mathrm{cm}^3$. The signal-to-noise ratio was somewhat poorer for the INLET observations than for the other cases, but reasonably good intercorrelation results were obtained. This is indicated by the waveforms for the

Table 6. Intercorrelations with BOXCAR as master event.

(BOXCAR pP-P = 0.96 s, pP/P = 0.9, ψ_∞ = 13x10^{10} cm^3)

Event	NSTA	N_w	pP-P, s	pP/P	ψ_∞ (x10^{10} cm^3)
ALMENDRO	34	0.1445	0.95	0.7	7.78
BENHAM	30	0.0949	0.95	0.9	12.35
CAMEMBERT	33	0.0979	1.00	0.9	9.33
CHESHIRE	28	0.1569	0.95	0.9	4.12
COLBY	26	0.0760	1.00	1.0	13.43
ESTUARY	22	0.0898	0.95	1.2	4.38
FONTINA	28	0.0662	0.95	0.8	11.97
GREELEY	38	0.0787	0.95	1.0	10.47
HALFBEAK	28	0.1987	0.90	1.1	5.41
HANDLEY	33	0.0690	0.95	0.9	17.87
INLET	29	0.2247	0.95	0.9	3.68
JORUM	35	0.0552	0.95	0.9	13.26
KASSERI	28	0.1009	0.95	0.9	11.28
MAST	38	0.2460	0.95	0.8	4.77
MUENSTER	27	0.2212	1.15	0.8	9.95
PIPKIN	25	0.3117	0.90	0.7	1.28
POOL	24	0.1461	0.95	0.9	5.61
PURSE	33	0.2399	0.90	1.0	2.25
RICKEY	25	0.2614	0.85	0.8	2.69
SCOTCH	29	0.1248	0.95	0.9	2.14
SLED	30	0.2116	0.90	0.7	3.62
STILTON	31	0.2546	0.85	0.6	2.85
STINGER	29	0.2899	0.85	0.9	1.64
TYBO	38	0.1807	0.95	0.8	5.59
FAULTLESS	42	0.1293	0.95	1.1	13.23
COMMODORE	34	0.1759	0.95	1.1	3.80
PILEDRIVER	23	0.2774	0.90	0.8	1.42

INLET : GREELEY intercorrelation shown in Fig. 13. The results of all of the intercorrelations with INLET as the master event are listed in Table 7. The absolute level of the ψ_∞ estimates is generally closer to that for the SCOTCH intercorrelations than to the BOXCAR results. With INLET or SCOTCH as master events, the ψ_∞ predicted for BOXCAR is about

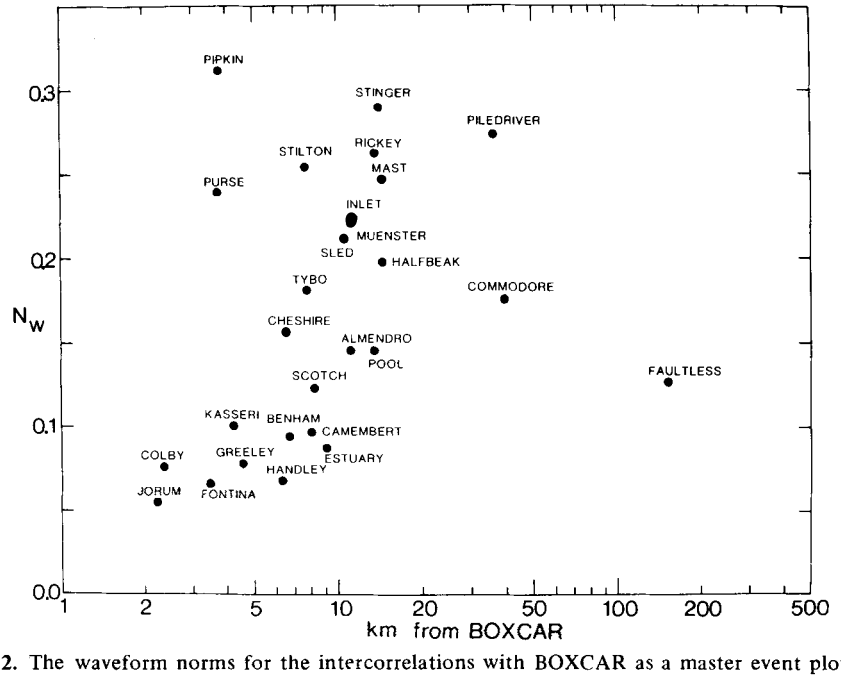

Figure 12. The waveform norms for the intercorrelations with BOXCAR as a master event plotted as a function of separation distance between the intercorrelated events.

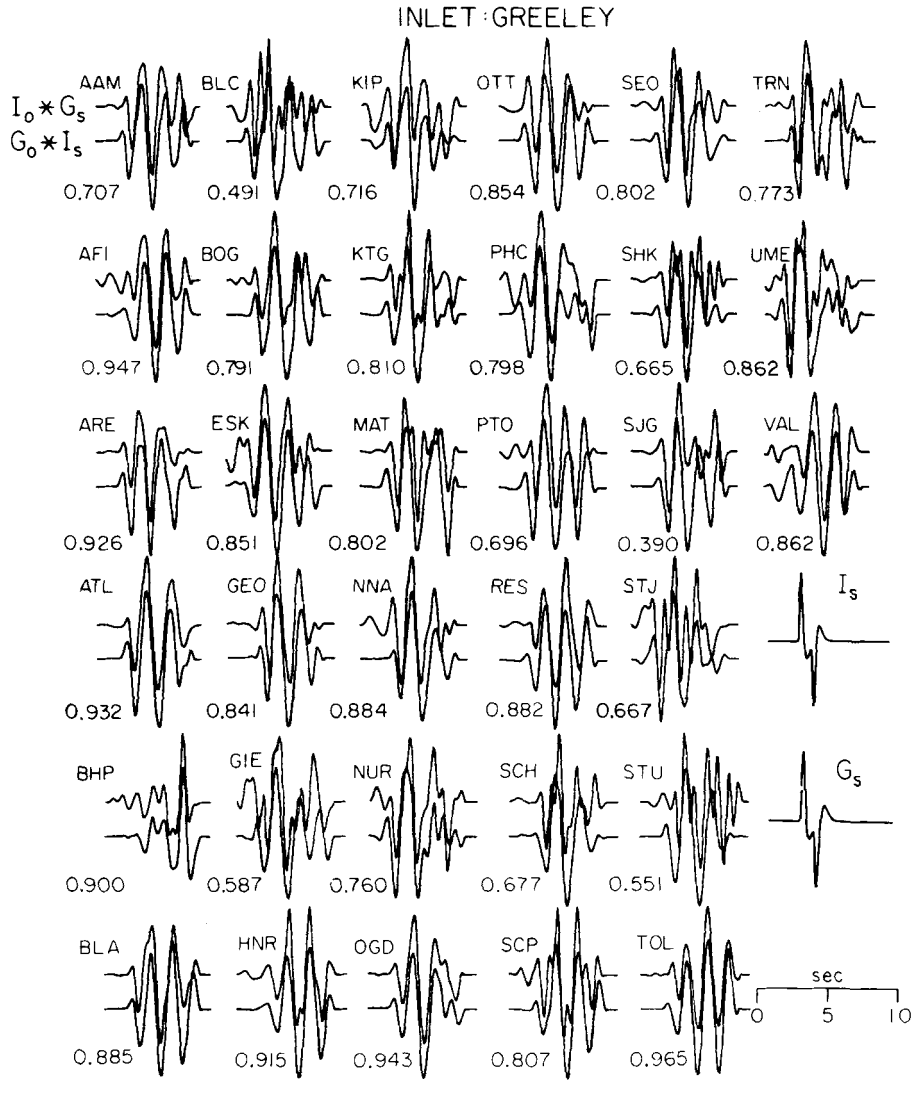

Figure 13. Intercorrelation of INLET and GREELEY for the optimal *pP* parameters given in Table 7. The conventions are the same as in Fig. 6. $K = 9$ for INLET and $K = 7.5$ for GREELEY.

6.0, less than 1/2 the value found in the near-field modelling. However, this discrepancy is close to that implied by the difference in t^* estimated from forward modelling of the average teleseismic amplitudes, which is 0.15 s larger for BOXCAR. This indicates that the near-field results may be biased for BOXCAR, or possibly the teleseismic amplitudes are anomalously low. Since the intercorrelation method provides relative source strength estimates, the relative values of ψ_∞ can still be compared between the master events. Similar to the SCOTCH intercorrelations, the INLET intercorrelations with ESTUARY, MUENSTER, COMMODORE, and STINGER result in anomalous *pP* parameters. It was discussed at length in Paper 1 that these are not necessarily the true *pP* parameters, because inadequacies in the source parameterization are compensated by apparent *pP* parameters. However, the intercorrelation technique is sensitive to relative differences in *pP* parameters, and

Table 7. Intercorrelations with INLET as master event.

(INLET pP-P = 0.90 s, pP/P = 0.9, $\psi_\infty = 3.0 \times 10^{10}$ cm^3)

Event	NSTA	N_w	pP-P, s	pP/P	ψ_∞ ($\times 10^{10}$ cm^3)
ALMENDRO	29	0.1727	1.00	1.1	4.57
BENHAM	24	0.2215	1.05	0.8	7.21
BOXCAR	28	0.2093	1.00	1.1	5.99
CAMEMBERT	31	0.2429	1.05	0.8	5.57
CHESHIRE	29	0.2345	1.00	1.0	2.17
COLBY	28	0.2359	1.10	1.1	7.03
ESTUARY	25	0.1927	1.00	1.4	2.22
FONTINA	29	0.2121	1.05	0.8	6.68
GREELEY	33	0.2149	1.00	0.9	5.77
HALFBEAK	25	0.1604	0.85	1.3	2.84
HANDLEY	29	0.1867	1.05	0.9	10.46
JORUM	29	0.1838	1.00	1.1	6.68
KASSERI	26	0.1898	0.95	0.8	7.00
MAST	38	0.1914	0.85	1.0	2.86
MUENSTER	26	0.2273	1.20	0.6	6.57
PIPKIN	25	0.2212	0.80	1.0	0.75
POOL	26	0.1565	0.95	1.2	2.99
PURSE	32	0.1674	0.80	1.3	1.22
RICKEY	23	0.1576	0.75	1.1	1.68
SCOTCH	26	0.1849	0.95	1.1	1.07
SLED	28	0.1257	0.85	1.1	1.97
STILTON	36	0.1871	0.80	1.1	1.51
STINGER	28	0.1854	0.80	1.4	0.87
TYBO	36	0.1755	0.90	1.2	3.00
FAULTLESS	33	0.2182	0.90	1.3	5.68
COMMODORE	30	0.3106	1.00	1.5	1.65
PILEDRIVER	22	0.3075	0.85	0.8	0.78

since most events have small differences in *pP* amplitude from that assumed for the master event, large differences do indicate anomalous waveform characteristics. With INLET as a master event, the waveform norms do not have a clear dependence on source separation, and the *pP* delays correlate quite well with burial depth.

The intercorrelations with MAST as the master event tended to have the largest waveform mismatches. This may reflect the location of MAST near the north-eastern edge of the Mesa (Fig. 1). The MAST source parameters used were: pP–P = 0.9 s, $|pP|/|P| = 0.9$, $K = 8$, $B = 1$, $\psi_\infty = 4.3 \times 10^{10}$ cm^3. Fig. 14 shows the intercorrelated waveforms for the optimal MAST : GREELEY intercorrelation. Note that the cross-correlation coefficients tend to vary more and are generally lower than for the other master event intercorrelations with GREELEY. The results for all 27 intercorrelations with MAST as a master event are listed in Table 8. The ψ_∞ values are generally similar to those found using SCOTCH and INLET as master events, and the BOXCAR value is again about a factor of 2 lower than the near-field result. ESTUARY and MUENSTER have anomalous *pP* parameters, as do HALFBEAK and POOL. MAST had the largest number of observations of the four master events, and more than 28 station pairs were intercorrelated for each event, with over 1050 waveforms being utilized to obtain the results in Table 8. There is a weak tendency for the closest events (such as STINGER and HALFBEAK) to have lower waveform norms, while more distant events (COMMODORE and PILEDRIVER) have significantly larger waveform norms. The *pP* delays also tend to be slightly larger than those found for the other master events, indicating that a shorter *pP* delay for MAST may be appropriate.

Comparison of ψ_∞ and relative amplitude measurements

The source strength estimates presented in Tables 4, 6, 7 and 8 are absolute estimates, but they are dependent upon the accuracy of each master event ψ_∞. As noted previously

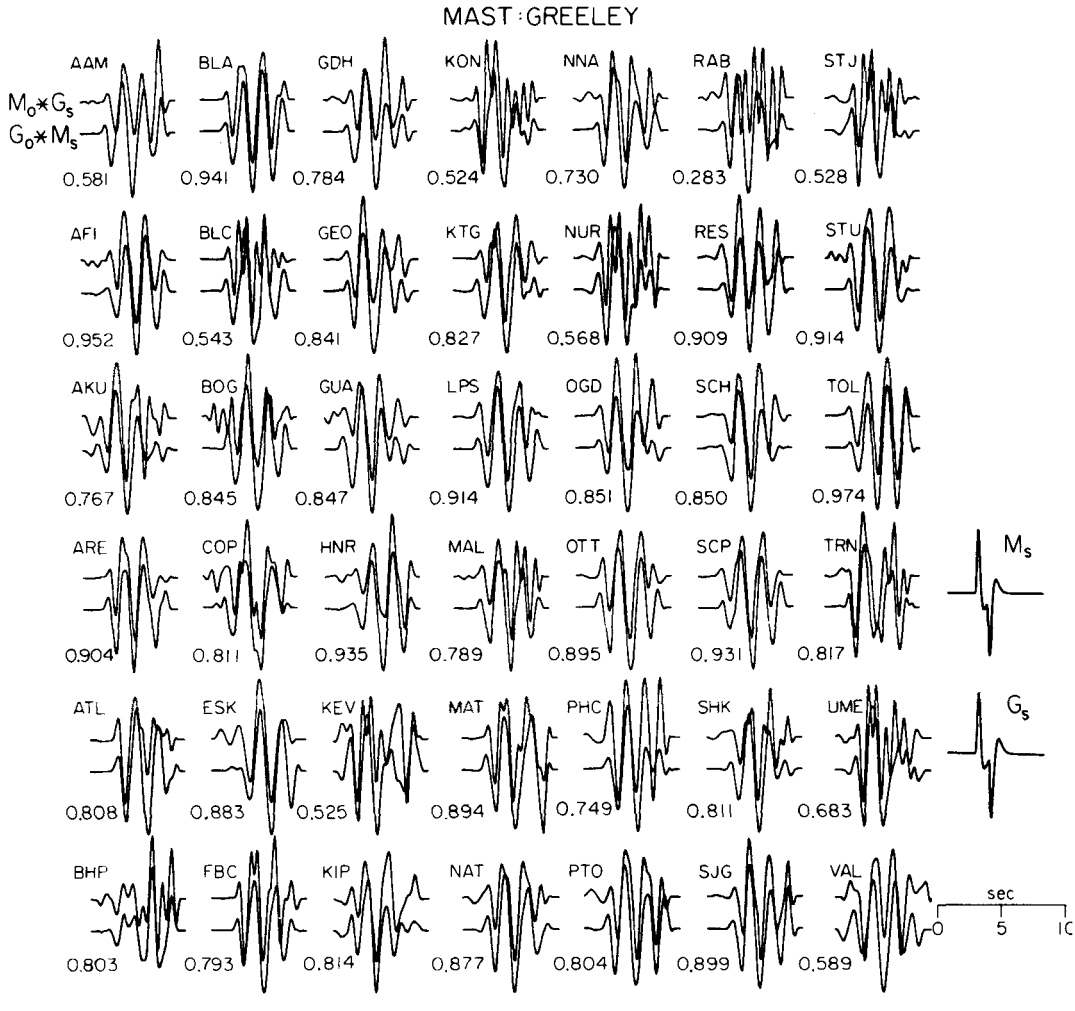

Figure 14. Intercorrelation of MAST and GREELEY for the optimal *pP* parameters given in Table 8. The conventions are the same as in Fig. 6. $K = 8$ for MAST and $K = 7.5$ for GREELEY.

BOXCAR appears to have too large a ψ_∞ compared with the other three master events. This probably results from contamination of the near-field records for BOXCAR. Since the ψ_∞ values are still accurately determined relative to each master event, their comparison is facilitated by dividing each by the ψ_∞ found or assumed for BOXCAR. These ratios are listed in Table 9. The consistency of the majority of the ψ_∞ estimates is readily apparent, though there are a few events for which the different master events give different relative values. In order to combine the results for different master events to obtain 'average' relative ψ_∞ determinations, a least squares procedure was used. Multiplicative factors were found for each master event that simultaneously minimize the scatter in the four ψ_∞ estimates for each of the 25 Pahute Mesa events. The multiplicative factors are then removed to combine the results for the different master events. This frees the ψ_∞ estimates from dependence on the master event ψ_∞s but no longer necessarily gives the true ψ_∞ levels. The output of the inversion is shown in Fig. 15, where the estimates for different master events have different symbols. As expected, the adjustments between SCOTCH, MAST and INLET were small,

Table 8. Intercorrelations with MAST as master event.

(MAST pP-P = 0.90 s, pP/P = 0.9, $\psi_\infty = 4.3 \times 10^{10}$ cm^3)

Event	NSTA	N_w	pP-P, s	pP/P	ψ_∞ ($\times 10^{10}$ cm^3)
ALMENDRO	39	0.1593	1.00	1.2	5.02
BENHAM	34	0.2958	1.10	0.9	7.66
BOXCAR	38	0.2108	1.10	1.2	7.75
CAMEMBERT	40	0.2412	1.15	0.9	6.97
CHESHIRE	36	0.2436	1.10	1.1	2.69
COLBY	37	0.2935	1.10	1.1	7.48
ESTUARY	33	0.1985	1.05	1.5	2.75
FONTINA	37	0.2579	1.15	1.0	6.76
GREELEY	42	0.2147	1.10	1.0	7.37
HALFBEAK	34	0.1084	0.85	1.5	3.25
HANDLEY	41	0.2220	1.10	1.0	11.5
INLET	38	0.1942	0.95	1.0	2.52
JORUM	40	0.1896	1.00	1.2	7.55
KASSERI	35	0.1893	1.05	0.9	8.59
MUENSTER	35	0.2415	1.25	0.8	7.76
PIPKIN	34	0.2166	0.80	0.8	0.80
POOL	35	0.1662	1.00	1.4	3.16
PURSE	41	0.1605	0.85	1.2	1.33
RICKEY	28	0.1546	0.75	1.0	1.71
SCOTCH	34	0.1606	1.00	1.2	1.30
SLED	35	0.1604	0.85	1.1	2.06
STILTON	46	0.1663	0.85	0.9	1.85
STINGER	33	0.1417	0.75	1.2	1.12
TYBO	47	0.1634	0.90	1.3	3.01
FAULTLESS	45	0.2002	0.95	1.2	8.20
COMMODORE	40	0.2607	1.00	1.5	1.97
PILEDRIVER	28	0.2854	0.90	1.1	0.85

Table 9. Relative source strengths.

$\psi_\infty / \psi_\infty$ BOXCAR

Master Event:	SCOTCH	BOXCAR	INLET	MAST	COMBINED
Event					
ALMENDRO	0.724	0.599	0.763	0.648	0.679
BENHAM	1.149	0.950	1.203	0.989	1.065
BOXCAR	1.000	1.000	1.000	1.000	1.000
CAMEMBERT	0.788	0.718	0.929	0.900	0.830
CHESHIRE	0.424	0.317	0.362	0.347	0.346
COLBY	1.053	1.033	1.174	0.966	1.015
ESTUARY	0.324	0.337	0.370	0.355	0.346
FONTINA	0.782	0.921	1.115	0.872	0.919
GREELEY	0.892	0.805	0.963	0.952	0.900
HALFBEAK	0.515	0.416	0.474	0.419	0.454
HANDLEY	1.478	1.375	1.746	1.482	1.511
INLET	0.387	0.283	0.500	0.325	0.368
JORUM	1.022	1.020	1.116	0.973	1.030
KASSERI	0.946	0.868	1.169	1.109	1.017
MAST	0.576	0.367	0.477	0.555	0.491
MUENSTER	0.925	0.766	1.096	1.002	0.940
PIPKIN*	0.126	0.099	0.124	0.103	0.112
POOL	0.425	0.431	0.500	0.408	0.439
PURSE*	0.222	0.173	0.204	0.172	0.192
RICKEY*	0.239	0.207	0.280	0.221	0.235
SCOTCH	0.239	0.164	0.178	0.168	0.186
SLED*	0.338	0.278	0.328	0.266	0.301
STILTON*	0.263	0.219	0.253	0.238	0.242
STINGER*	0.174	0.126	0.145	0.145	0.147
TYBO*	0.519	0.430	0.501	0.388	0.457
FAULTLESS	1.055	1.018	0.948	1.059	
COMMODORE	0.228	0.292	0.275	0.254	
PILEDRIVER	0.120	0.109	0.130	0.109	

* ψ_∞ estimates should be increased by 1.19 to account for near-source velocity structure.

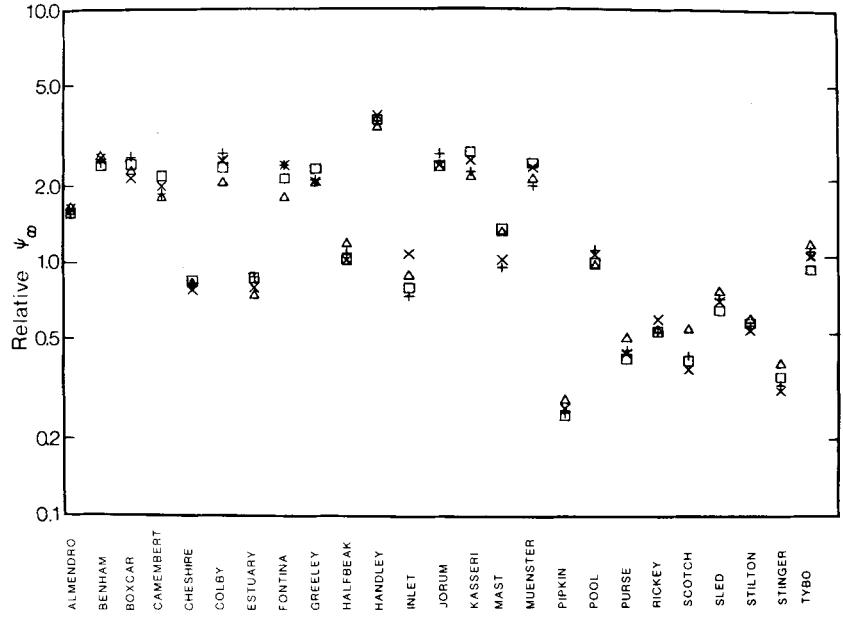

Figure 15. The results of a least squares inversion used to combine the estimates from the different master event intercorrelations. The estimates for each master event are distinguished by boxes (MAST), X's (INLET), triangles (SCOTCH), and pluses (BOXCAR).

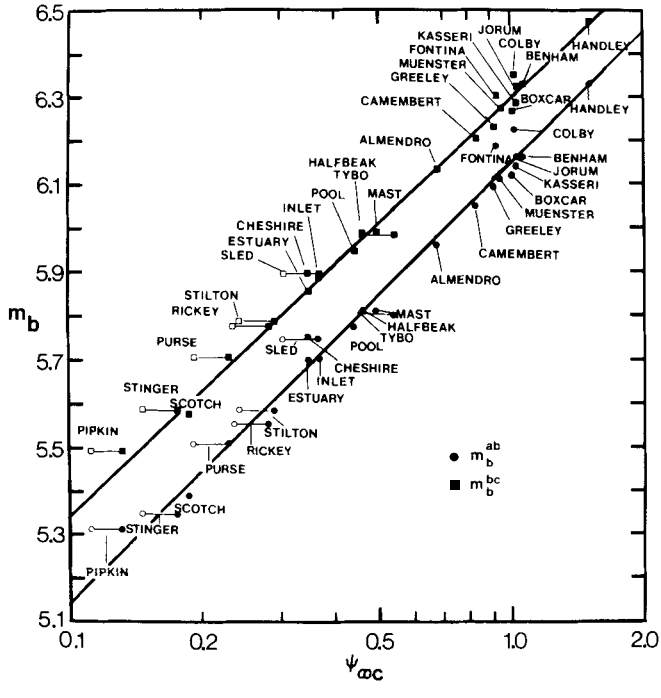

Figure 16. Comparison of m_b^{ab} and m_b^{bc} values from Table 1 with the normalized relative source strengths, $\psi_{\infty c}$ from the combined master event inversion (Table 9), with (filled symbols) and without (empty symbols) source velocity corrections for the shallow events. The curves are for the regressions in equation (10).

while the BOXCAR adjustment was larger. The averages of these values for each event are considered to be our best relative ψ_∞ estimates. These averages were divided by the average for BOXCAR and are also listed in Table 9. No weighting was applied in the inversion, though reasonable weighting schemes would employ the number of observations for each intercorrelation and the residual waveform norm. The non-Pahute Mesa events were not included in this inversion.

The normalized relative source strength estimates from the combined inversion, $\psi_{\infty c}$ (Table 9), are plotted against m_b^{ab} and m_b^{bc} in Fig. 16. It is clear that the relative amplitude and intercorrelation results are quite consistent. Events SCOTCH, SLED, FONTINA and COLBY show the largest relative mismatches. The $\psi_{\infty c}$ values are shown with and without corrections for the depth dependence of the *P*-wave excitation, which exists if the source velocity increases over the range of burial depths. This was not originally allowed for in the intercorrelation analysis. The Pahute Mesa near-surface velocity model of Hartzell *et al.* (1983) indicates a *P*-wave velocity increase of from 2.8 to 3.3 km s^{-1} at a depth of 0.8 km. Thus, the ψ_∞ estimates for the seven events buried at depths less than 0.8 km (Table 1) could be increased by a factor of 1.19. Fig. 16 illustrates the effect of this correction, which tends to increase the slope between amplitude and ψ_∞ measurements. In all cases the relative scatter is reduced, with the exception of TYBO. TYBO was buried at a depth of 0.765 km, which is very close to the 0.8 km interface, so perhaps the correction is not appropriate for this case. The actual velocity structure may be a gradient rather than a localized increase, so there is some uncertainty in the precise correction to make. Note that SCOTCH and SLED no longer deviate from the general trends. Variance weighted regressions with the revised $\psi_{\infty c}$ provide the following relations,

$$\log (ab) = (2.69 \pm 0.01) + (0.921 \pm 0.027) \log \psi_{\infty c}$$

$$\log (bc) = (2.85 \pm 0.01) + (0.883 \pm 0.021) \log \psi_{\infty c}$$

$$\log \frac{(A^{ab})}{T} = (2.77 \pm 0.01) + (0.961 \pm 0.029) \log \psi_{\infty c}$$

$$\log \frac{(A^{bc})}{T} = (2.94 \pm 0.01) + (0.922 \pm 0.019) \log \psi_{\infty c}$$

$$m_b^{ab} = (6.15 \pm 0.01) + (1.011 \pm 0.026) \log \psi_{\infty c}$$

$$m_b^{bc} = (6.30 \pm 0.01) + (0.950 \pm 0.018) \log \psi_{\infty c}. \qquad (10)$$

While the slopes are all close to unity, the closest is for m_b^{ab}. Applying period corrections in the amplitude measurement increases the linearity between the amplitude and ψ_∞ estimates. This reflects the large range in yield of the events and the discernible shifts in dominant period. The m_b^{ab} values differ from the A^{ab}/T results principally in the slight differences in station weighting due to the different spreading corrections and logarithmic averaging. It appears that m_b^{ab} provides the best agreement with the intercorrelation results, if a linear relation with ψ_∞ is reasonable.

The question arises as to whether we should really expect a linear relation between m_b^{ab} and ψ_∞. This should only be true if the period correction in the magnitude calculation accounts completely for the change in K with yield. The increase in slope observed between the *ab* and m_b^{ab} regressions suggests that this is at least partially occurring. It is of course important to emphasize that this agreement is only expected for events with *pP* delays long enough to permit a clean measure of the direct *P* amplitude. The *pP* effect on the *bc* type measurements clearly tends to decrease the slope for the lag times involved. It is possible for

Table 10. Empirical yield estimates (Kt) from amplitude measurements.

Event	Announced	Dahlman and Israelson	ab	bc	$\frac{A^{ab}}{T}$	$\frac{A^{bc}}{T}$	m_b^{ab}	m_b^{bc}
ALMENDRO		570	737	731	641	656	665	683
BENHAM	1150	1000	1090	1120	1032	1087	1177	1232
BOXCAR	1300	1000	1001	973	949	951	1051	1045
CAMEMBERT		750	855	829	786	788	869	852
CHESHIRE		350	406	372	378	353	369	334
COLBY		900	1341	1216	1218	1174	1418	1329
ESTUARY		350	314	302	324	315	310	297
FONTINA		900	1118	983	1103	1020	1272	1145
GREELEY	870	830	870	833	871	868	958	936
HALFBEAK	365	450	455	482	427	459	431	458
HANDLEY		1900	1648	1499	1635	1585	1952	1868
INLET		500	363	371	333	340	318	322
JORUM		700	1034	1033	1044	1084	1187	1214
KASSERI		1200	1056	999	1007	986	1123	1090
MAST		520	459	472	430	451	425	442
MUENSTER		600	1032	1050	915	965	1016	1060
PIPKIN		82	110	111	125	123	103	101
POOL		500	443	438	398	398	390	387
PURSE		180	187	199	202	212	179	189
RICKEY		300	232	266	228	257	207	237
SCOTCH	155	140	151	151	150	149	129	127
SLED		260	379	366	369	357	358	337
STILTON		275	251	268	249	266	226	240
STINGER		160	118	137	137	156	113	131
TYBO		380	434	443	425	439	427	433
COMMODORE	250		273	261	289	281	280	294
FAULTLESS	1200		842	1002	961	1160	1248	1572
PILEDRIVER	56		146	138	156	148	136	116

the opposite trend to occur if the lag times are short enough. At any rate, it is very encouraging that the results are in good agreement for the Pahute Mesa events, especially since the first 5 s of the P waveforms were used in determining the $\psi_{\infty c}$ estimates while only the first $^1/_2$ s is used to measure the ab amplitudes. This suggests that slapdown phases, anomalous pP behaviour, or other individual event complexity has not biased the intercorrelation results on average.

The yields of five of the Pahute Mesa events have been released. These are given in Table 10. Using these values, it is possible to make yield estimates for the rest of the events based on the amplitude and ψ_∞ measurements. Variance weighed regressions of the amplitude measurements on known yields give the following relations for the Pahute Mesa tests:

$$\log ab = (0.275 \pm 0.250) + (0.800 + 0.089) \log Y$$

$$\log bc = (0.488 \pm 0.284) + (0.782 \pm 0.102) \log Y$$

$$\log \frac{A^{ab}}{T} = (0.048 \pm 0.303) + (0.916 \pm 0.109) \log Y$$

$$\log \frac{A^{bc}}{T} = (0.315 \pm 0.310) + (0.876 \pm 0.111) \log Y$$

$$m_b^{ab} = (3.702 \pm 0.245) + (0.800 \pm 0.088) \log Y$$

$$m_b^{bc} = (3.951 \pm 0.267) + (0.769 \pm 0.096) \log Y. \qquad (11)$$

The yields for each event predicted by these relations are listed in Table 10, along with the relative amplitude based predictions of Dahlman & Israelson (1977). For several events, the latter source gives significantly different yield estimates, notably for ALMENDRO, COLBY,

FONTINA, INLET, JORUM, MUENSTER, and SLED. The yield estimates for the three non-Pahute Mesa tests are based on using the values in Table 1 and equations (11), though these events were not included in determining the yield relations.

A similar procedure was used to establish empirical relations between yield and the ψ_∞ estimates for each master event and the combined $\psi_{\infty c}$. The relations are:

$$\text{(SCOTCH) } \log \psi_\infty = (8.624 \pm 0.183) + (0.708 \pm 0.065) \log Y$$

$$\text{(BOXCAR) } \log \psi_\infty = (8.516 \pm 0.155) + (0.844 \pm 0.056) \log Y$$

$$\text{(INLET) } \log \psi_\infty = (8.190 \pm 0.269) + (0.860 \pm 0.096) \log Y$$

$$\text{(MAST) } \log \psi_\infty = (8.265 \pm 0.222) + (0.861 \pm 0.079) \log Y$$

$$\text{(COMBINED) } \log \psi_{\infty c} = (-2.589 \pm 0.214) + (0.860 \pm 0.076) \log Y. \quad (12)$$

The event names identify the master event in each case. These yield-scaling relationships are for $B = 1$. The corresponding expression found in Paper 1 for the Amchitka events is

$$\text{(MILROW) } \log \psi_\infty = (8.93 \pm 0.01) + (0.728 \pm 0.001) \log Y. \quad (13)$$

It is important to note that both the baseline and the slope differ between the two test sites, which provides a strong motivation for using empirical relations between ψ_∞ and yield rather than existing scaling laws. The relatively low yield exponent for the SCOTCH results, compared with the other master events, suggests that there may be some contamination of SCOTCH, perhaps associated with its overburial. This, along with the variation in baseline between master events, indicates the importance of using several master events in the intercorrelation process, for no single event will be a perfect master event. The yield-scaling exponent of the BOXCAR, INLET, MAST and COMBINED results shows little scatter, and has a value close to the long-period theoretical scaling (Bache 1982):

$$\psi_\infty \simeq Y^{0.89}. \quad (14)$$

This suggests that, unlike for the Amchitka events, B does not vary significantly with yield for the Pahute Mesa tests, though it is not known whether $B = 1$ is appropriate or not.

Yield estimates based on the empirical ψ_∞-yield scaling relations above, using the source velocity corrections, are given in Table 11. The estimates in Tables 10 and 11 are generally quite compatible, though the intercorrelation results tend to be smaller for CHESHIRE, HALFBEAK, PIPKIN, PURSE and SLED. While formal uncertainties are hard to specify, it appears that both relative amplitude and intercorrelation techniques have about 15–25 per cent error bounds. Surprisingly, the intercorrelation results are remarkably successful at predicting the non-Pahute Mesa event yields. Events that tended to have anomalous pP parameters, such as ESTUARY, HALFBEAK and MUENSTER, do not have obviously anomalous yield estimates. The empirical approach adopted frees all of these estimates from any bias due to incorrect ψ_∞ values of the master events, but the combined inversion results are considered to be the 'preferred' yield estimates from the intercorrelation analysis.

The consistently poor waveform agreement for the different master event intercorrelations with events PIPKIN, STILTON and PILEDRIVER leads us to expect that the yield estimates for these events are relatively poor. It is probable that the yield estimates for different master events are more accurate for events with yields close to that of the master event. For example, the low yield events may be more accurately predicted by the SCOTCH results, and the large yield events by the BOXCAR results. Also, one might expect that

Table 11. Empirical yield estimates (Kt) from intercorrelation.

		Master Event				
Event	Announced	SCOTCH	BOXCAR	INLET	MAST	COMBINED
ALMENDRO		675	650	743	673	653
BENHAM	1150	1296	1123	1263	1099	1103
BOXCAR	1300	1065	1194	1018	1114	1025
CAMEMBERT		761	806	935	986	825
CHESHIRE		253	306	312	326	298
COLBY		916	1241	1227	1070	1043
ESTUARY		217	329	320	335	299
FONTINA		753	1083	1156	950	929
GREELEY	870	906	924	975	1052	907
HALFBEAK	365	417	422	428	406	409
HANDLEY		1848	1740	1947	1759	1657
INLET		278	268	456	302	320
JORUM		1097	1222	1157	1080	1061
KASSERI		985	1009	1221	1256	1045
MAST		488	364	430	562	448
MUENSTER		954	870	1133	1116	953
PIPKIN		73	95	110	98	98
POOL		318	441	454	394	394
PURSE		162	184	197	176	184
RICKEY		180	226	283	236	233
SCOTCH	155	141	141	137	141	146
SLED		294	322	342	294	311
STILTON		206	242	252	258	241
STINGER		115	127	132	144	135
TYBO		540	539	558	454	504
COMMODORE	250	132	278	227	227	
FAULTLESS	1200	1074	1220	958	1190	
PILEDRIVER	56	53	87	95	85	

proximity to the master event influences the accuracy of the yield estimates. These considerations require knowledge of all of the actual yields and cannot be fully developed here.

The nature of anomalous events

The intercorrelation procedure provides analytical waveform comparisons allowing systematic differences in waveforms to be detected. These are manifested in azimuthal patterns in the correlations as seen in Fig. 10, and in anomalous average *pP* parameters. The waveform differences can often be detected in the raw data as shown in Fig. 17, where HALFBEAK and MUENSTER have large secondary arrivals. Given large data sets, it is possible to seek distance and azimuthal trends in these waveforms. Preliminary efforts along these lines have shown erratic patterns of *pP* amplitude predictions, but occasional azimuthal patterns of *pP* delays (Lay *et al.* 1984e), which may ultimately be related to the mechanism producing the anomaly.

The amplitude and waveform variations between Pahute Mesa events probably have several causes. The degree of coupling, free surface interaction, and deep structure of the Mesa probably vary from event to event. It is also known that the amount of tectonic release varies substantially between events. Lay *et al.* (1984b) have made an initial attempt to test whether there is a signature of tectonic release in the short-period *P*-waves from Pahute Mesa explosions. The long-period body wave and surface wave studies they review demonstrate that there was high stress drop, strike-slip tectonic release accompanying several Pahute Mesa events, particularly MUENSTER, BENHAM and GREELEY. The azimuthal variations of short-period *ab* amplitudes for Pahute Mesa events are consistent in orientation with the $\sin(2\phi)$ *P*-wave radiation patterns for the known tectonic release radiation. Events with large *F* factors were shown by Lay *et al.* (1984b) to have statistically better defined $\sin(2\phi)$ patterns. While such an azimuthal pattern could be caused by upper mantle velocity anomalies or receiver variations, the orientation and variation from event to event suggest

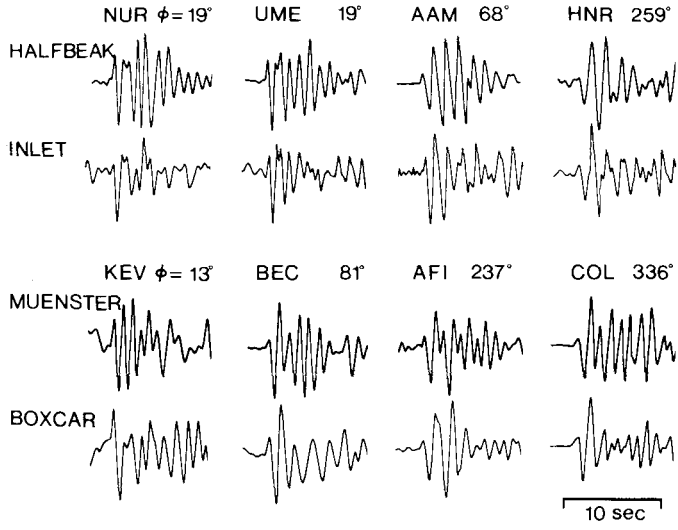

Figure 17. Comparison of observed short-period *P*-waves for HALFBEAK and INLET and MUENSTER and BOXCAR. Note the additional arrivals several seconds into the HALFBEAK and MUENSTER waveforms. This complexity is observed at a wide range of azimuths, but not at all stations.

the possibility that tectonic release is responsible. Such an explanation would require that all of the Pahute Mesa events are similarly affected.

While tectonic release may contribute to the Pahute Mesa amplitude pattern for all events, an important question for the intercorrelation procedure is whether the waveform variations are due to variable tectonic release. Fig. 18 compares the observations for the high tectonic release event GREELEY with the low tectonic release event COLBY, as a function

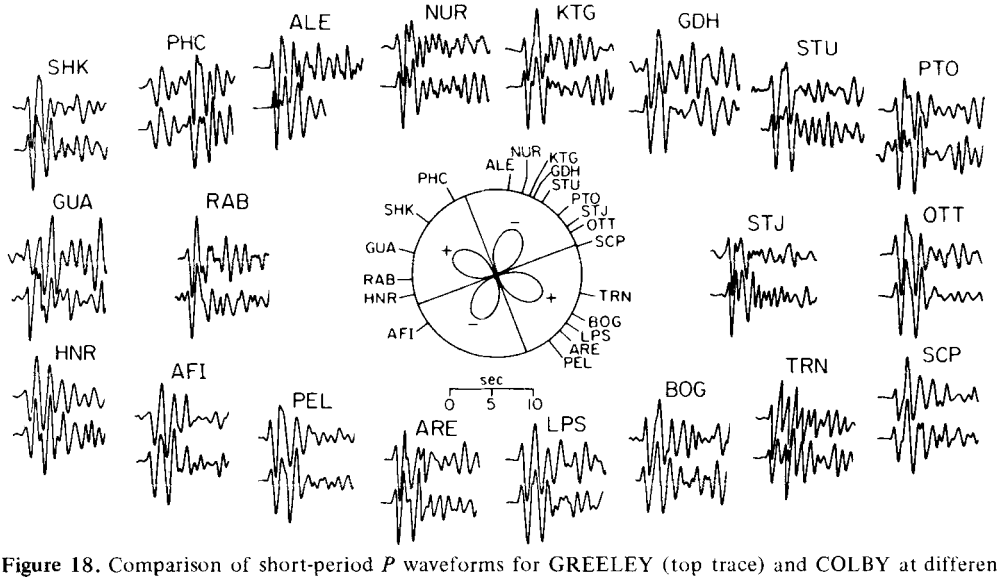

Figure 18. Comparison of short-period *P* waveforms for GREELEY (top trace) and COLBY at different azimuths from the source region. The azimuth of each station is indicated in the centre. Within the circle, the *P*-wave radiation pattern for the tectonic release orientation for GREELEY, as constrained by long-period observations, is shown. The negative lobes would be the quadrants with opposite polarity to the explosion arrival.

of azimuth around the double couple radiation pattern for GREELEY. If tectonic release does affect these waveforms, it must produce subtle effects. However, the synthetic calculations presented by Lay *et al.* (1984b) indicate rather subtle azimuthal variations in waveforms, particularly for finite source models. Given the additional complexities due to receiver functions, and the presence of some tectonic release for all Pahute Mesa events, the net effects of differential tectonic release could be very hard to detect. A systematic investigation of our intercorrelation results as a function of position within the Mesa, long-period F factors, and near-field observations of spall should throw light on these questions. At present we have not attempted to account for possible tectonic release contamination of the waveforms, but it is clear that only by a procedure like intercorrelation will we be able to quantitatively account for tectonic release if it does in fact affect events of interest.

Up to this point we have emphasized the Pahute Mesa results, since 90 per cent of our data is for those events. In both the amplitude (except when averaging the amplitudes) and intercorrelation analyses, we treated FAULTLESS, PILEDRIVER and COMMODORE as though they were additional Pahute Mesa events, just as one would initially treat foreign events close to but outside a well-studied test site. The intercorrelation results gave large residual waveform mismatches for COMMODORE and PILEDRIVER and anomalous pP amplitudes for COMMODORE. FAULTLESS generally intercorrelated well, and the yields were successfully predicted for all three events, despite these problems. The latter result appears to be rather fortuitous, for very large amplitude scatter was found for each intercorrelation.

The combined information in the waveform norms, pP parameters, and differences in azimuthal amplitude patterns between these events permits ready identification of the Pahute Mesa events as comprising a distinct test site from Yucca Flat, Climax Stock, and the FAULTLESS site. Since there are several events within the Mesa with equally high waveform mismatches, and with anomalous pP parameters, it appears that the azimuthal amplitude behaviour is critical to defining the distinct test site. This aspect is readily quantified in the intercorrelation analysis by computing the variance in each ψ_∞ estimate.

Conclusion

Intercorrelation analysis has been performed for a large number of NTS explosions. A large data set has been collected and processed with four objectives in mind: first, to establish a reasonable procedure for performing intercorrelation for a test site given detailed knowledge of only a few master events; second, to obtain source strength estimates for a large number of events to compare with other yield estimation procedures; third, to identify and characterize anomalous events; and finally, to establish the decision-making process for defining distinct test sites.

We have adopted a largely empirical approach to applying the intercorrelation analysis, maximizing the advantages of the limited information available for a master event. The crucial master event information is the yield, seismic source strength, and source function rise time. The latter two values have been shown to be obtainable from near-field strong motion recordings. After establishing the rise time parameter for other events by empirical relations or forward modelling, intercorrelation is performed to obtain ψ_∞ and pP parameter estimates. Given several known yields, empirical relations can be established to estimate yield, or scaling relations can be directly applied if they are independently confirmed. Careful monitoring of individual station and overall network intercorrelations provides important information on possible anomalies. Optimally, a large set of stations and several master events should be used.

Source estimates have been obtained by intercorrelation for 25 Pahute Mesa tests, along with carefully measured amplitude results. Similar estimates were found for three events outside of Pahute Mesa. Over 1200 waveforms were analytically analysed to obtain these estimates. The results for four master events have been compared and combined to give relative source strength estimates. The need for more than a single master event was made clear when one of the master events (BOXCAR) was found to be inconsistent in baseline with the other three. Comparison of the average amplitude measures with the source strength estimates obtained by intercorrelation provides strong support for the reliability of the waveform analysis. Application of source velocity corrections to the intercorrelation results leads to a linear relation between m_b^{ab} and ψ_∞ averages. This is the expected result for the Pahute Mesa events for which *pP* delays are so long that m_b^{ab} is not affected by the *pP* arrival. Yield estimates are presented for both the amplitude and intercorrelation results.

Some initial progress has been made on understanding the nature of anomalous events detected by the intercorrelation analysis. A critical aspect of detecting and characterizing anomalous events is good azimuthal station coverage. Azimuthal variations in the original traces and individual intercorrelation norms and *pP* parameters are generally observed for anomalous events. Further detailed inspection of the *pP* variations will shed light on the complex free surface interaction. The possible effects of tectonic release on Pahute Mesa events have been considered. While a reasonable tectonic release model may account for some of the azimuthal variation in *ab* amplitudes, which have a clear $\sin(2\phi)$ pattern, the waveform effects must usually be small and similar from event to event.

On the basis of intercorrelations and amplitude comparisons between Pahute Mesa events and FAULTLESS, COMMODORE and PILEDRIVER, it has been possible to identify the events within Pahute Mesa as belonging to a distinct test site (except for a few anomalous events). Both waveform differences and relative amplitude variations are used as criteria for defining a distinct test site, with the latter providing the most robust diagnostic.

Acknowledgments

This research was supported by the Advanced Research Projects Agency of the Department of Defense and was monitored by the Air Force Office of Scientific Research under contract number F49620-83-C-0051. I thank Larry Burdick and Don Helmberger for discussions on this project and Rob Van der Voo and two anonymous reviewers for reviewing the manuscript. Cindy Arvesen performed the prodigious task of collecting and digitizing the majority of the data. The manuscript was typed by Marie Schatz and Martha Sweigert.

References

Bache, T., 1982. Estimating the yield of underground nuclear explosions, *Bull. seism. Soc. Am.*, 72, S131–S168.

Bache, T. C., Day, S. M. & Savino, J. M., 1979. Automated magnitude measures, earthquake source monitoring, VFM discriminant testing and summary of current research, *Techn. Rep. SSS-R-79-3933,* S-cubed, La Jolla, California.

Baumgardt, D. R., 1983. Teleseismic *P*-coda stability and coda-magnitude yield estimation, *Proc. 5th Annual DARPA/AFOSR Symp. Seismic Detection, Analysis, Discrimination, Yield Determination,* 77–78, Darpa, Arlington, Virginia.

Burdick, L. J., Wallace, T. & Lay, T., 1984. Modeling near-field and teleseismic observations from the Amchitka test site, *J. geophys. Res.*, 89, 4373–4388.

Butler, R. & Ruff, L., 1980. Teleseismic short period amplitudes: source and receiver variations, *Bull. seism. Soc. Am.*, 70, 831–850.

Dahlman, O. & Israelson, H., 1977. *Monitoring Underground Nuclear Explosions,* Elsevier, New York.

Frasier, C., 1972. Observations of *pP* in the short-period phases of NTS explosions recorded at Norway, *Geophys. J. R. astr. Soc.*, **31**, 99–109.

Hartzell, S. H., Burdick, L. J. & Lay, T., 1983. Effective source functions for Pahute Mesa nuclear tests, *Final Techn. Rep. WCCP-R-83-3*, Woodward-Clyde Consultants, Pasadena, California.

Kraft, G; D., Griffin, J. N. & Baumgardt, D. R., 1982. A comparative evaluation of several magnitude measures in the time and frequency domains for nuclear explosion yield estimation (abstract), *Earthq. Notes*, **53**, 7.

Kulhanek, O., 1971. *P*-wave amplitude spectra of Nevada underground nuclear explosions, *Pure appl. Geophys.*, **88**, 121–136.

Langston, C. A. & Helmberger, D. V., 1975. A procedure for modelling shallow dislocation sources, *Geophys. J. R. astr. Soc.*, **42**, 117–130.

Lay, T., Burdick, L. J. & Helmberger, D. V., 1984a. Estimating the yields of the Amchitka tests by waveform intercorrelation, *Geophys. J. R. astr. Soc.*, **78**, 181–207.

Lay, T., Wallace, T. C. & Helmberger, D. V., 1984b. The effects of tectonic release on short period *P* waves from NTS explosions, *Bull. seism. Soc. Am.*, **74**, 819–842.

Lay, T., Burdick, L. J., Helmberger, C. V. & Arvesen, C. A., 1984c. Estimating seismic yield and defining distinct test sites using complete waveform information, *Final Techn. Rep., WCCP-R-84-01*, Woodward-Clyde Consultants, Pasadena, California.

Lay, T., Helmberger, D. V. & Harkrider, D. G., 1984d. Source models and yield-scaling relations for underground nuclear explosions at Amchitka Island, *Bull. seism. Soc. Am.*, **74**, 843–862.

Lay, T., Arvesen, C., Burger, R. & Burdick, L., 1984e. Estimating seismic yield and defining distinct test sites, using complete waveform information, *Semi-Annual Techn. Rep. WCCP-R-84-03*, Woodward-Clyde Consultants, Pasadena, California.

Marshall, P. D., 1972. Some seismic results from a world-wide sample of large underground explosions, *AWRE, Rep. 049/72*, United Kingdom Atomic Energy Authority.

Mellman, G. R. & Kaufman, S. K., 1981. Relative waveform inversion, *Techn. Rep. SGI-R-81-048*, Sierra Geophysics, Inc., Redmond, Washington.

Mueller, R. A. & Murphy, J. R., 1971. Seismic characteristics of underground nuclear detonations. Part I. Seismic spectrum scaling, *Bull. seism. Soc. Am.*, **61**, 1675–1692.

Murphy, J., 1977. Seismic source functions and magnitude determinations for underground nuclear detonations, *Bull. seism. Soc. Am.*, **67**, 135–158.

Ringdal, F., 1983. Magnitudes from *P* coda and L_g using NORSAR data, *Proc. 5th Annual DARPA/AFOSR Symp. Seismic Detection, Analysis, Discrimination, Yield Determination*, p. 34, DARPA, Arlington, Virginia.

Shapira, A. & Kulhanek, O., 1978. Conventional and spectral short-period body-wave magnitudes, *Bull. seism. Soc. Am.*, **68**, 1195–1198.

Springer, D. L., 1974. Secondary sources of seismic waves from underground nuclear explosions, *Bull. seism. Soc. Am.*, **64**, 581–594.

Veith, K. F. & Clawson, G. E., 1972. Magnitudes from short period *P* wave data, *Bull. seism. Soc. Am.*, **62**, 435–452.